NASA Technical Memorandum 105347

The Aerodynamic Effect of Fillet Radius in a Low Speed Compressor Cascade

Brian P. Curlett
Lewis Research Center
Cleveland, Ohio

November 1991

NASA

THE AERODYNAMIC EFFECT OF FILLET RADIUS IN A LOW SPEED COMPRESSOR CASCADE

Brian P. Curlett
National Aeronautics and Space Administration
Lewis Research Center
Cleveland, Ohio 44135

Introduction

In most cases, a finite fillet size is required for structural integrity in both rotating and non-rotating blade rows. The size of this fillet is usually minimized because increasing fillet radius will decrease aerodynamic performance due to increasing profile drag. However, the addition of a fillet between an airfoil and hub or shroud will reduce the interaction between the end wall and blade boundary layers. The result is a thinner boundary layer in the corner region that is less likely to separate. This is similar to the use of a fillet in a wing/fuselage intersection. In addition to modifying the behavior of the three-dimensional boundary layer in the corner, the fillet will change the blade loading and possibly influence the roll up of secondary vortices. It has not been previously determined if fillet geometry will have a positive or negative influence on corner or channel vortices formed in a cascade channel. The effect of fillet size on these vortices and the corner flow separation is examined in this paper.

Brockett and Kozak [1] have looked at the influence of fillet size in axial flow turbine stators, experimentally. Their results show that small fillets, with a radius of about 5 percent chord, increased thermodynamic efficiency by 1.4 percent over the case with zero fillet radius. A fillet radius of 10 percent chord was found to have only a slightly lower efficiency than the smaller fillet and still a significant improvement over the zero fillet case. They speculate that the increase in efficiency was due to the fillet limiting corner flow separation and that the larger fillet did not continue to increase efficiency because of the additional profile drag. A 1.4 percent increase in efficiency is fairly significant improvement in a turbine stator. Compressors may realize even more

of an improvement because pressure gradients in a compressor are less favorable and, therefore, corner flow separation is even a greater problem.

Other researchers have found that larger fillet size could possibly increase losses. Stratford [2] has shown in a compressor cascade the addition of a fillet increased the size of the separation region and the losses. However, his testing only included one blade type, British standard C4 blades of 10% maximum thickness, at one set of flow conditions.

Tweedt and Okiishi [3] have investigated the influence of fillet size on stator performance in a two-stage, axial-flow compressor using double circular arc blades. Their results did not show any sizable effects due to the fillet. Tweedt's results did indicate that the larger fillet size produced lower losses near the casing end wall. This is most likely due to the fillet limiting flow separation in the corner.

Some previous research has indicated that the application of high concentrations of dihedral (or leaning) of the blade towards the end walls will reduce secondary flow losses. In his paper, DeParvine [4] compares losses of blades with straight, circular and elliptical stacking lines. The elliptical stacking of the blade profiles, causing the high concentration of dihedral angle near the end wall, produces the lowest losses. However, this type of blade loading slightly increases the losses at midspan. From these results it can be hypothesized that using a large fillet will give the same benefit as the elliptically stacked blades while achieving lower losses near the blade midspan.

The present experiment was designed to help clarify the aerodynamic influences of fillet size in a compressor cascade. A large test matrix was used in order to accomplish this. Cascades were tested with two blade types, double circular arc and controlled diffusion, over a large range of incidence angles. Three fillet sizes, 0, 7.5 and 15 percent chord, and two boundary layer thickness were used in the experiment.

Symbols

BL1	thin boundary layer case
BL2	thick boundary layer case
DF	diffusion factor
KE	kinetic energy
P_0	total pressure
q	dynamic pressure
Q	arbitrary quantity
u	pitchwise component of velocity in the exit plane
v	spanwise component of velocity in the exit plane
V	velocity
W	weighting factor
x	pitchwise coordinate
y	spanwise coordinate measured from side wall
z	streamwise coordinate
α	pitch angle from axial (degrees)
θ	yaw angle from axial (degrees)
ρ	density
σ	solidity
ω	total pressure loss coefficient
Ω_z	streamwise vorticity
< >	ensemble average

Subscripts

1	cascade inlet condition
2	cascade exit condition
MS	midspan
θ	pitchwise direction

The Experiment

Experimental Facility

Data were collected in the C1 cascade tunnel at the von Karman Institute for Fluid Dynamics in Rhode Saint Genese, Belgium. This facility is shown schematically in Figure 1 and photographically in Figures 2 and 3. The facility is driven by a 18 KW DC motor connected to a centrifugal blower. The blower pumps air into a large settling chamber with screens to reduce the turbulence level. The air then enters a contraction to a rectangular test section of 127x500 mm.

The test section is equipped with a suction slot, 21.5 cm upstream of the cascade center. The suction slot is used for boundary layer removal when two-dimensionality is important. It was not used in the current study because of the desirability of having thicker boundary layer and the interest in the three-dimensionality of the flow.

The test section is equipped with two motorized traverse mechanisms for flow measurement, one upstream and one downstream of the cascade.

Instrumentation

A NACA short prism pressure probe was used to measure inlet flow conditions. This probe could measure static pressure, total pressure and pitch angle. The NACA probe was located 12 cm in front of blade center at midspan and could be traversed in the pitchwise direction.

The downstream data were collected with a two head, 5-hole pressure probe, shown in Figures 3 and 4. One head is a shielded total pressure probe (Kiel probe) and the other head consists of 4 holes arranged to measure pitch and yaw angles. The 4-hole head is less then 1 mm in diameter. This probe was calibrated in the exit plane of the C1 cascade tunnel with the cascade blades removed. A pitch/yaw range of ±30 degrees was used. The calibration procedure is described in [5]. Static pressure at the cascade exit was assumed to be ambient pressure for the purpose of calculating velocity. The probe

was positioned at a 4 degree yaw angle to allow closer movement to the side wall without interference from the probe support. A test of the calibration indicates that angles could be measured with an uncertainty of ±1.5 degrees.

A third pressure measurement was made in the settling chamber before the inlet contraction with a Kiel probe. This pressure was monitored during the test so that tunnel pressure variations could be corrected. Large drifts (>0.5 mm H_2O) in tunnel pressure were corrected manually by adjusting the motor rpm. Smaller variations in tunnel pressure were corrected during data reduction by using the following formula:

$$P_i' = P_i P_{set} / P_{meas.}$$

where:
P_i' = corrected pressures from the 5-hole probe (i=1..5)
P_i = measured pressures from the 5-hole probe (i=1..5)
P_{set} = desired tunnel pressure setting
$P_{meas.}$ = measured tunnel pressure in the settling chamber

Pressures were measured with a set of six Validyne variable reluctance pressure transducers. The transducers were calibrated to a range of 140 mm H_2O = 2.44 volts (or 2000 bits). Outputs of the transducers were connected to integrating circuits to remove high frequency fluctuations with integrating constants of 0.1 sec. Data were then sent to an IBM PC/AT compatible computer using a MetraByte 12 bit analog-to-digital converter. Data sampling was externally triggered from the traverse mechanism at every millimeter of probe movement.

Blade Geometry

Two blade profiles were used in the testing: a double circular arc (DCA) and a controlled diffusion (CD) blade. Blade profiles are shown in Figure 5. Both blades have the same chord, maximum thickness, solidity, and stagger angle. The coordinates of the controlled diffusion blades were taken from [6] and are not repeated here. The DCA blades were designed using NACA correlations [7] to do equivalent turning to the CD

blades. Cascade parameters are given in Table 1. Each cascade consists of ten blades.

Three fillet radii of 0, 7.5 and 15.0 mm were used during the testing. The relative size of these fillets can be seen in the photograph in Figure 6. The 7.5 mm fillet radius, or 7.5 percent chord, is approximately the standard size. This fillet size is also approximately the size of fillet required to prevent corner flow separation based on the theory of Debruge [8,9].

Double circular arc blade	
chord	100 mm
pitch	60 mm
span	127 mm
maximum thickness-to-chord ratio	0.07
stagger angle	14.2 deg
camber angle	49.6 deg
leading edge radius	0.42 mm
trailing edge radius	0.42 mm
design inlet angle	40.0 deg
Controlled diffusion blade	
chord	100 mm
pitch	60 mm
span	127 mm
maximum thickness-to-chord ratio	0.07
stagger angle	14.2 deg
setting angle	14.4 deg
leading edge radius	0.90 mm
trailing edge radius	1.24 mm
design inlet angle	40.0 deg

Table 1: Cascade Parameters

Blades were manufactured on a 3-axis numeric control machine using a spherical cutter. The cutter has a radius equal to the fillet radius, therefore, the cutter was stopped short of full span movement leaving the desired fillet size. Surfaces were then lightly sanded by hand to provide a smoother finish. Blades were manufactured out of ureol, a plastic-like material.

Measurements

Measurements were made 1 cm downstream in a plane parallel to the blades' trailing edges, as shown in Figure 7. Thirteen spanwise measurement locations were used. The locations are: 1.5, 3.5, 6.0, 8.5, 11.0, 13.5, 18.5, 23.5, 28.5, 33.5, 43.5, 53.5 and 63.5 mm from the side wall. The measurement locations are shown graphically in Figure 8. At each measurement location 180 samples, one every 1 mm, were acquired over the 3 central blade pitches. At each measurement location pitch angle, yaw angle and total pressure were calculated using the calibration data from the 5-hole pressure probe.

Data Reduction

Performance Properties

Using downstream flow measurements along with results from the upstream traverse the total pressure loss coefficient can be calculated as:

$$\omega(x,y) = \frac{(\overline{P_{01}})_{MS} - P_{02}}{(\overline{q_1})_{MS}}$$

where $(\overline{P_{01}})_{MS}$ and $(\overline{q_1})_{MS}$ are the pitchwise averaged total and dynamic pressure measured by the upstream probe at midspan, respectively. These local values of loss coefficient are plotted as contours over the exit plane of the cascade. This proved to be a very useful method for analyzing the flow field.

The diffusion factor, DF, is calculated at the blade midspan, for each test case, using the expression:

$$DF = 1 - \frac{\overline{V_2}}{V_1} + \frac{\overline{V_{\theta 1}} - \overline{V_{\theta 2}}}{2\sigma V_1}$$

Integrated Quantities

To determine the global properties of the flow field it is necessary to reduce the data into simpler parameters. This can be done by averaging the data over the exit plane. The average value of a parameter Q(x,y) is given by:

$$\bar{\bar{Q}} = \frac{\int_{y_1}^{y_2}\int_{x_1}^{x_2} Q(x,y)\,W(x,y)\,dxdy}{\int_{y_1}^{y_2}\int_{x_1}^{x_2} W(x,y)\,dxdy}$$

where x and y are the pitchwise and spanwise directions, respectively, and W(x,y) is a weighting factor. For an area averaged quantity the weighting factor W(x,y) is 1.0 and for a mass averaged quantity W(x,y) is $\rho V_2 \cos(\alpha_2)\cos(\theta_2)$.

The variation of some of the quantities in the pitchwise direction are also important. The pitchwise average value of a quantity is given by:

$$\overline{Q}(y) = \frac{\int_{x_1}^{x_2} Q(x,y)\,W(x,y)\,dx}{\int_{x_1}^{x_2} W(x,y)\,dx}$$

These averaging techniques are used for: pressures, velocities and loss coefficients.

Streamwise Vorticity Calculation

Streamwise vorticity was calculated from the downstream flow measurements by evaluating derivatives of cubic splines fit to the u (pitchwise) and v (spanwise) components of velocity. The velocity components are defined by:

$u = V_2 \sin(\alpha_2) \cos(\theta_2)$

$v = V_2 \cos(\alpha_2) \sin(\theta_2)$

The differentiation of experimental data is always difficult because small fluctuations in the data can result in large gradients. For this reason the components of velocity were first phase averaged over the three pitches where data were available. The phase averaging will smooth the data, as well as help complete the grid where the data did not converge. (Non-convergence in calculating the velocity vector is caused by a turbulent fluctuation resulting in a the velocity vector outside the calibration range.) The phase (or ensemble) average for the 180 points in one traverse can be represented by the following equation:

$$\langle u \rangle_i = (u_i + u_{i+60} + u_{i+120})/3 \qquad (\text{for } i = 1..60)$$

The u component velocity was fit in the spanwise direction and the v component of velocity was fit in the pitchwise direction with cubic splines. The spatial derivatives $\partial\langle u \rangle/\partial y$ and $\partial\langle v \rangle/\partial x$ were then evaluated at each grid point by taking the derivative of the cubic equation at that point. The streamwise vorticity is then:

$$\langle \Omega_z \rangle = \frac{\partial \langle v \rangle}{\partial x} - \frac{\partial \langle u \rangle}{\partial y}$$

Results

Inlet Flow Conditions

The tunnel plenum pressure was set to 126 mm H_2O for all of the test cases. This resulted in a Reynolds number variation from 300,000 to 350,000 as the inlet flow angle was varied. The Reynolds number is based on the inlet velocity to the cascade and the chord length.

The inlet turbulent intensity was measured using a hot-wire probe located at midspan, 120 mm in front of the central blade. Results are given in Table 2.

Two inlet boundary layer thicknesses were used during the test. One was the natural boundary layer that developed on the side wall, BL1, and the other was an artificially thickened boundary layer, BL2. The thick boundary layer case was used only with the double circular arc blade type. The boundary layer was thickened by using vortex generators placed on the side walls just after the inlet contraction, 1.35 m upstream of the central blade. The vortex generators were closely spaced triangles, 6 mm in height and 5 mm at the base. Inlet boundary layer profiles were measured using a boundary layer total pressure probe in place of the NACA short prism inlet probe. Figure 9 shows the boundary layer profiles. Other boundary layer parameters are given in Table 2.

Table 2: Test Conditions

	BL 1	BL 2
displacement thickness (mm)	1.929	3.717
momentum thickness	1.613	3.288
inlet turbulent intensity	0.014	0.021
diffusion factor (design condition)	0.33	0.30
axial velocity ratio (design condition)	1.11	1.14

CD Blade Performance

The overall performance of a cascade can best be evaluated from the mass averaged total pressure loss coefficient. The total pressure loss coefficient is shown in Figure 10 as a function of inlet flow angle for the CD blade with thin boundary layer. These results indicate that, for the controlled diffusion blade, the addition of a fillet increased losses as much as 28 percent over the zero fillet case. The only improvement in loss coefficient over the zero fillet case was at the highest incidence tested. This high incidence is outside the normal operating range of the compressor and the flow is completely separated on the blade.

Figures 11 and 13 show total pressure loss contours in the downstream plane parallel to the trailing edge of the cascade, at blade design condition and at the stall condition, respectively. These figures indicate that most of the losses occur in the corner between the blade suction side and the end wall. The accumulation of low energy air at this location is due to (i) the movement of the side wall boundary layer from the pressure side to the suction side corner and (ii) separation of the three-dimensional boundary layer in the corner. Note in Figure 11, the greater losses in the wake of the larger fillet. Also, note the movement of the high loss contour lines towards the blade midspan as the size of the fillet is increased. This implies an increase in the size of the separation zone. These findings are in agreement with the findings of Stratford [2].

The distribution of losses over the blade span, Figure 15, indicates that the addition of the fillet has increased losses over most of the blade span. This distribution of losses over the blade span can be better evaluated by plotting the pitchwise averaged loss coefficient minus the inlet boundary layer loss coefficient and the "2D" blade loss (or midspan loss). These results are shown in Figure 16. Again, the zero fillet case has lower losses over most of the span. Although, near the side wall the zero fillet case had measurably higher losses. This may be due to the weaker corner vortex for the zero fillet case which carries high energy air into the sidewall boundary layer.

The location of maximum loss in Figure 16 corresponds to the location of the

corner vortex. This can easily be seen by comparing Figure 16 with the vorticity contour in Figure 17. The higher losses, for the finite fillet cases, at the vortex location may indicate a stronger corner vortex.

Three additional quantities were calculated to help support this hypothesis. These quantities are: (i) peak vorticity in the flow field, (ii) averaged vorticity over the flow field and (iii) total kinetic energy of the flow *not* in the mean flow direction. (i) is simply the level of vorticity found in the core of the vortex on the vorticity contour map, (ii) is the area average of the absolute value of vorticity, and (iii) is the area average of KE_{loss}, where:

$$KE_{loss} = \tfrac{1}{2}\rho[(u-V_2\sin(\alpha_2))^2 + v^2]$$

Note that KE_{loss} is not a measure of lost energy. It is a measure of energy that is not in the mean flow direction and, therefore, may not be recovered to do practical work. This "loss" is not included in the total pressure loss coefficient because the total pressure probe was shielded and, therefore, insensitive to flow angle.

All of the above mentioned quantities follow the same trend for the controlled diffusion blade. That is, they all increase with increasing fillet size. Table 3 shows these results at the design inlet flow angle, data are non-dimensionalized by the zero fillet case. This suggests that for this type of blade the fillet size should be made as small as possible in order to keep secondary flow losses to a minimum. One possible explanation for this is that the fillet provides a smooth transition as the side wall boundary layer moves across the channel and starts to roll-up the side of the blade.

Fillet Size	0.00	7.50	15.0
Peak Vorticity	1.00	1.38	3.50
Average Vorticity	1.00	1.03	1.23
KE_{loss}	1.00	1.07	1.09

Table 3: Losses, CD Blade, α_1=40.0 deg.

It was also found that the larger trailing edge radius, caused by the addition of the fillet, increases losses in the wake. This can be seen in Figures 12 and 14 which shows the velocity distribution in the same plane as the losses contours of Figures 11 and 13. Notice in Figure 12 (bottom) the large acceleration of air from the end wall pressure corner (x=30mm) to the wake region behind the fillet. The flow of air from the pressure side corner to the fillet wake was observed for all test conditions having large fillet radii.

DCA Blade Performance

Thin Boundary Layer

The double circular arc blade configuration results are not as clear as the CD blade case. There was no clear trend in the total losses measured at low to moderate incidence, Figure 18. As the incidence angle was increased, however, the cascades with finite fillet radii have measurably lower losses. Figures 19 through 24 show loss contours and velocity vectors at incidence angles of 37, 46 and 52 degrees, respectively. It appears that the addition of the fillet helps decrease the size of the separated region at high incidence. This can be observed in the loss contours, Figure 21. Note that the wake is thinner and the size of the separation region is smaller for the 15 mm fillet case then for the zero fillet case. The thinning of the wake may be an effect of the increasing axial-velocity-ratio (V_{a2}/V_{a1}). This causes a squeezing of the boundary layer and reduces the size of the separation. The axial-velocity-ratio increases with fillet size because of the decrease in channel area. The AVR for the 0, 7.5 and 15 mm fillet radii at α_1=53 were found to be 1.11, 1.15 and 1.20. That is an 8 percent increase in AVR from the zero fillet case to the 15 mm fillet case.

The spanwise distribution of loss coefficient for the three fillet radii are shown in Figure 25. The losses at blade midspan are greater for the zero fillet case, however, near the end wall the zero fillet case has lower losses. This is the exact opposite of what occurred in the CD cascade. The fact that losses increase with fillet radius near the end wall is not surprising because of the thick trailing edge of the blade in this region. The

high losses for the zero fillet case at the blade midspan is more difficult to explain. Trends in the vorticity levels are not as clear as for the CD cascade. The large differences in the results found indicate that blade loading is an important factor in the aerodynamic role of the fillet.

Thick Boundary Layer

Test for the thick boundary layer case were only done for the zero and 15 mm fillet sizes. It was felt that this would be adequate to demonstrate any boundary layer effects. Results indicate that the thick boundary layer case behaves very similarly to the thinner boundary layer case. Results are shown in Figures 26-30. Again, the loss contours indicate that the reversed flow area decreases and the wake thins as the fillet radius is increased.

Note the crossing of the lines on the total pressure loss coefficient plot in Figure 26 is the same as that in Figure 18. This gives more confidence in the results that at first, look like possible experimental error. The crossing of the lines in these figures is difficult to explain and will require additional research.

As in the thin boundary layer case the velocity vector plots, Figures 28 and 30 show sudden acceleration of the flow in the trailing edge region of the fillet. In order to reduce this loss, it may be advisable to decrease the size of the fillet towards the trailing edge.

Conclusions

The addition of a fillet in the corner between the blade and side wall increased secondary flow and profile losses for the CD blades tested. Results clearly indicate, that for this configuration, fillet size should be made only large enough for structural integrity.

The fillet was not found to significantly change losses at low to moderate incidence angles for the double circular arc blades. However, as the incidence angle was increased the cascades with finite fillet radii were found to have measurably lower losses. This means that the usable incidence range for the double circular arc blades can be slightly extended by the use of a fillet. The experimental data show the same trends regardless of the inlet boundary layer thickness. The most important conclusion for the cascade with double circular arc blades is that the use of a fillet will not degrade the cascade performance. This means that structure designers will not have to worry about the aerodynamic effects when selecting a structurally appropriate fillet size.

References

1. BROCKETT,W., KOZAK, A. Small axial turbine stator technology program. NASA CR-165602, April 1982.

2. STRATFORD, B. The prevention of flow separation and reversal in the corners of compressor blade cascades. Aeronautical Journal, vol. 77, pp 249-256.

3. TWEEDT,D., OKIISHI, T. Stator blade row geometry modification influence on two-stage compressor aerodynamic performance. AFOSR-TR-84-0418, December 1983.

4. DEPARVINE, R. The effects of dihedral on secondary flow in a low speed turbine cascade. VKI PR 1988-06.

5. SHEPPERD, I.C. A four hole pressure probe for fluid measurement in three dimensions. J. Fluids Engineering (ASME), Vol. 103, No. 4, October 1981, pp 590-594.

6. ELAZAR, Y. A mapping of the viscous flow behavior in a controlled diffusion compressor cascade using laser doppler velocimetery and preliminary evaluation of codes for the prediction of stall. Doctoral Thesis, Navy Postgraduate School, Monterey, California, March 1988.

7. NASA Special Publication 36, *Aerodynamic Design of Axial Flow Compressors*, edited by Irving A. Johnsen and Robert O. Bullock, 1965.

8. DEBRUGE, L.L. The aerodynamic significance of fillet geometry in turbocompressor blade rows. J. Engineering for Power (ASME), Vol. 102, October 1980, pp 984-993.

9. DEBRUGE, L.L. Determination of aerodynamically adequate fillet geometry in turbocompressor blade rows. AFWAL-TR-81-2020, May 1981.

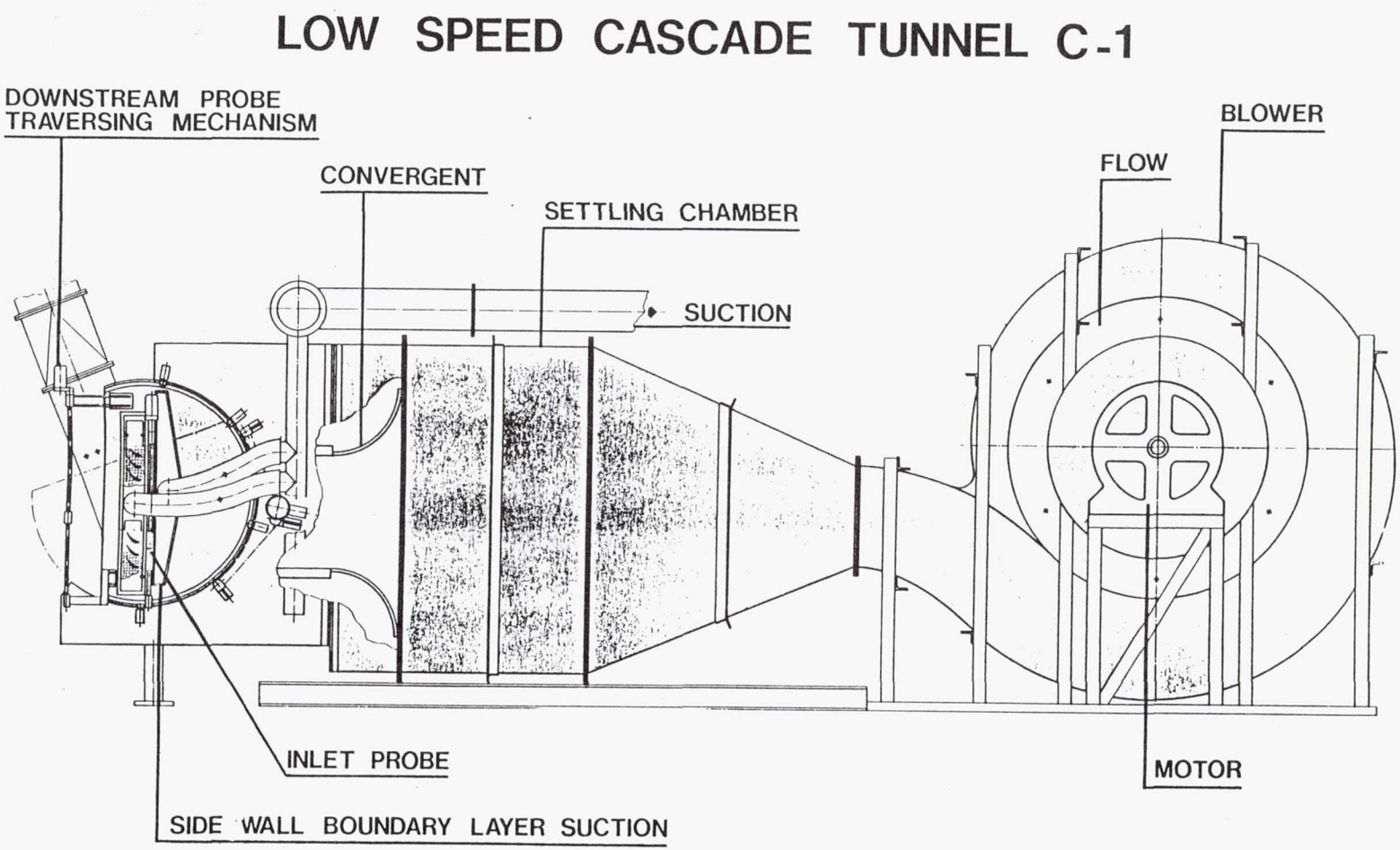

Figure 1: C1 Cascade Tunnel

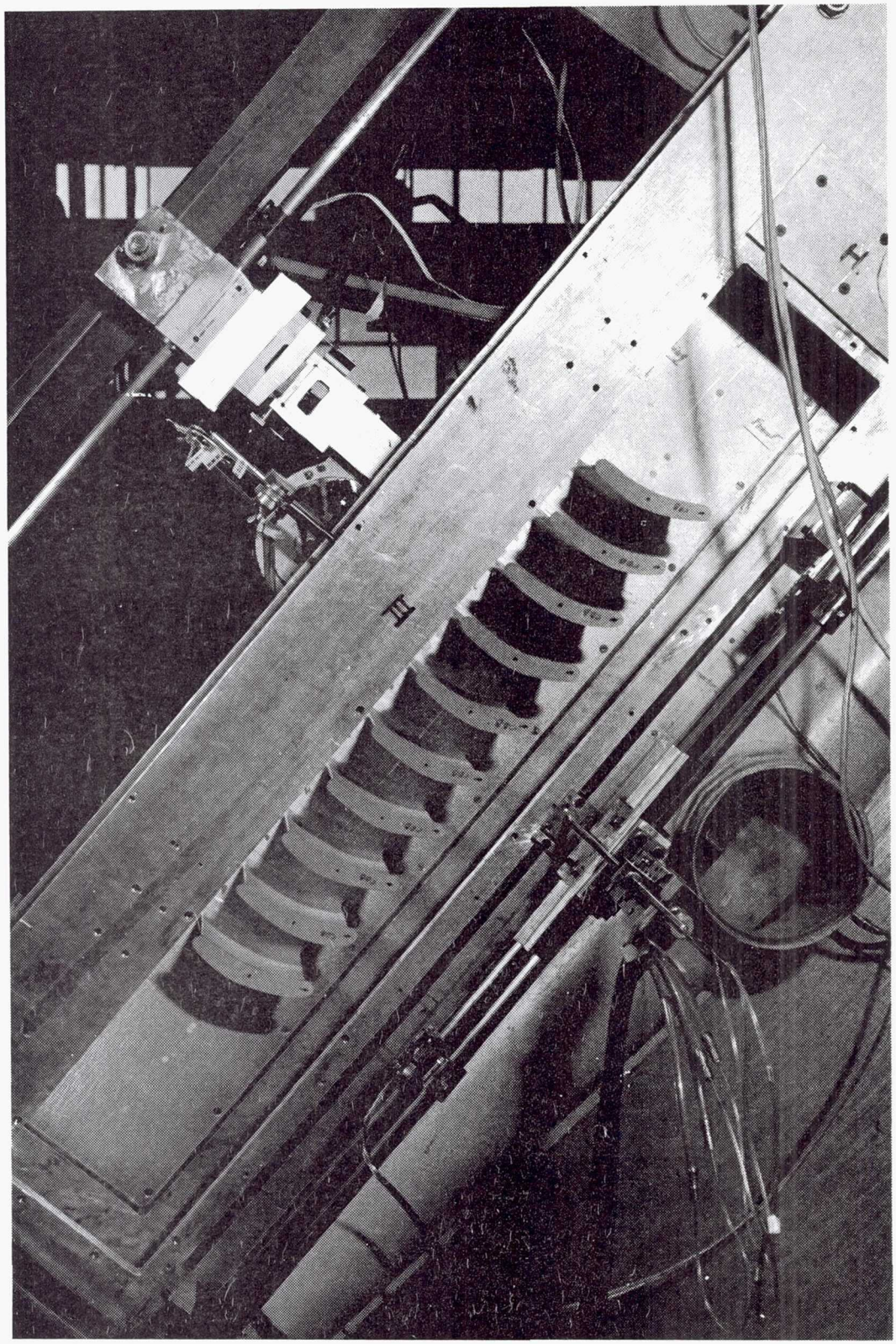

Figure 2: C1 Cascade Tunnel with side wall removed.

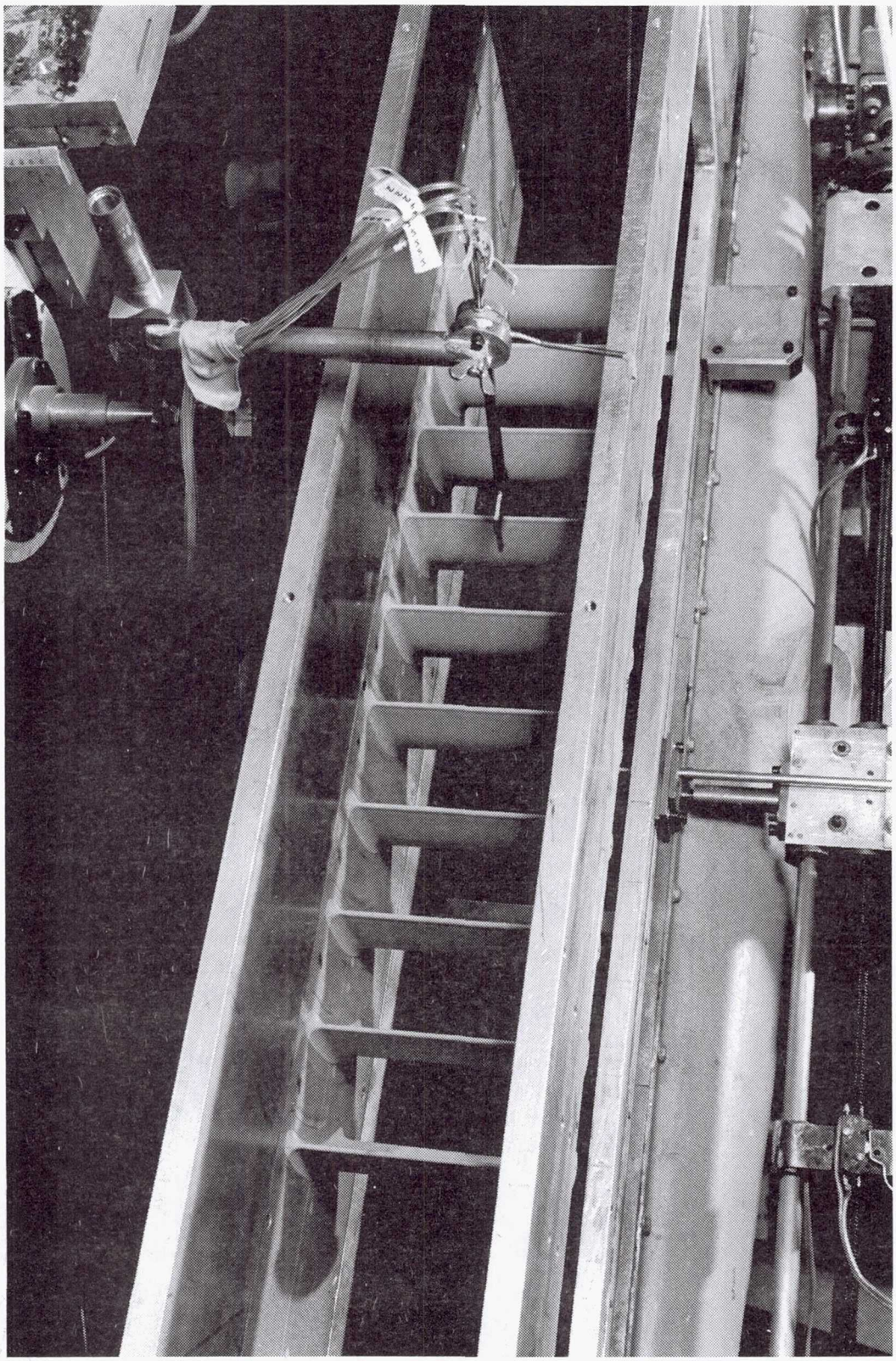

Figure 3: Exit plane of the C1 Cascade Tunnel.

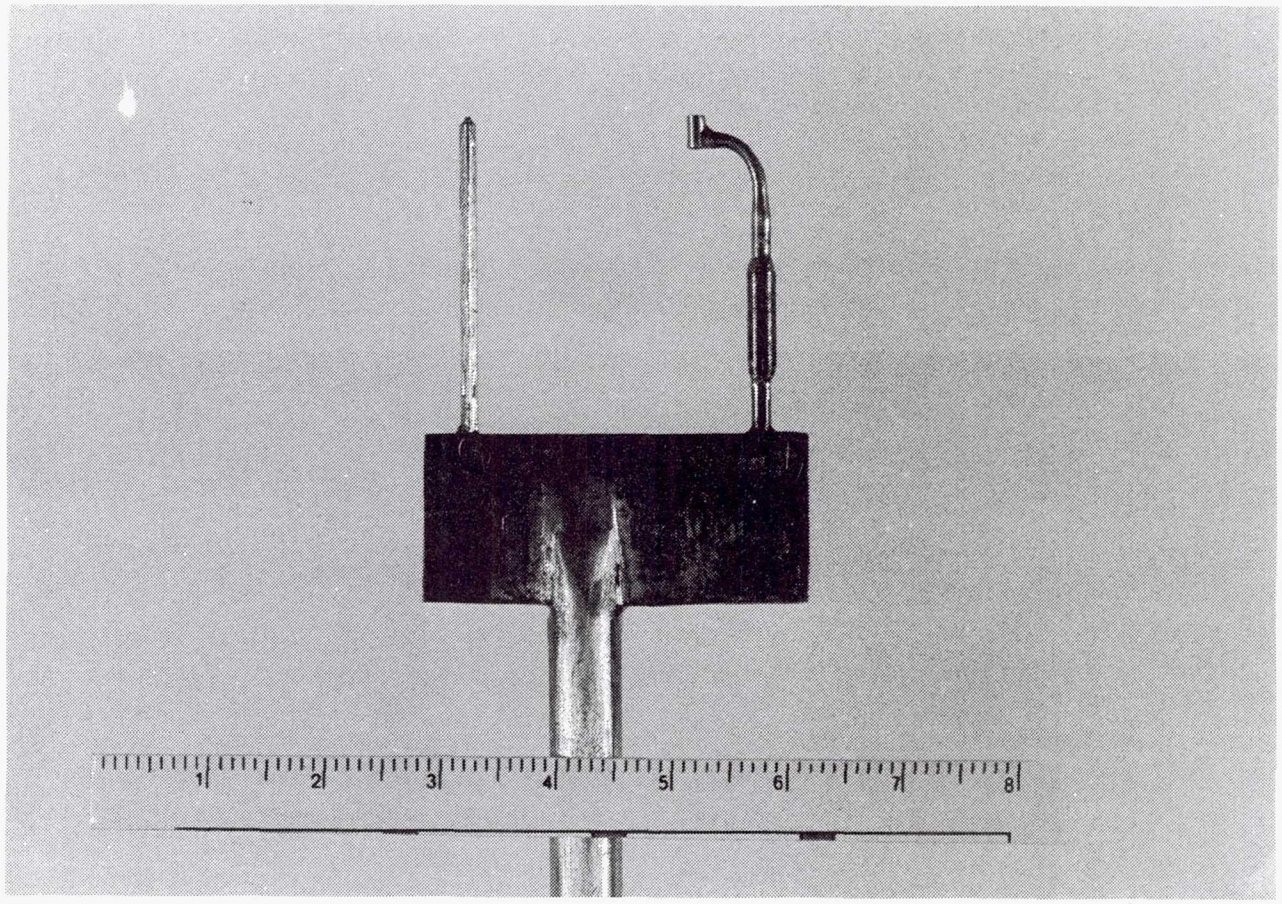

Figure 4: 5-Hole Probe.

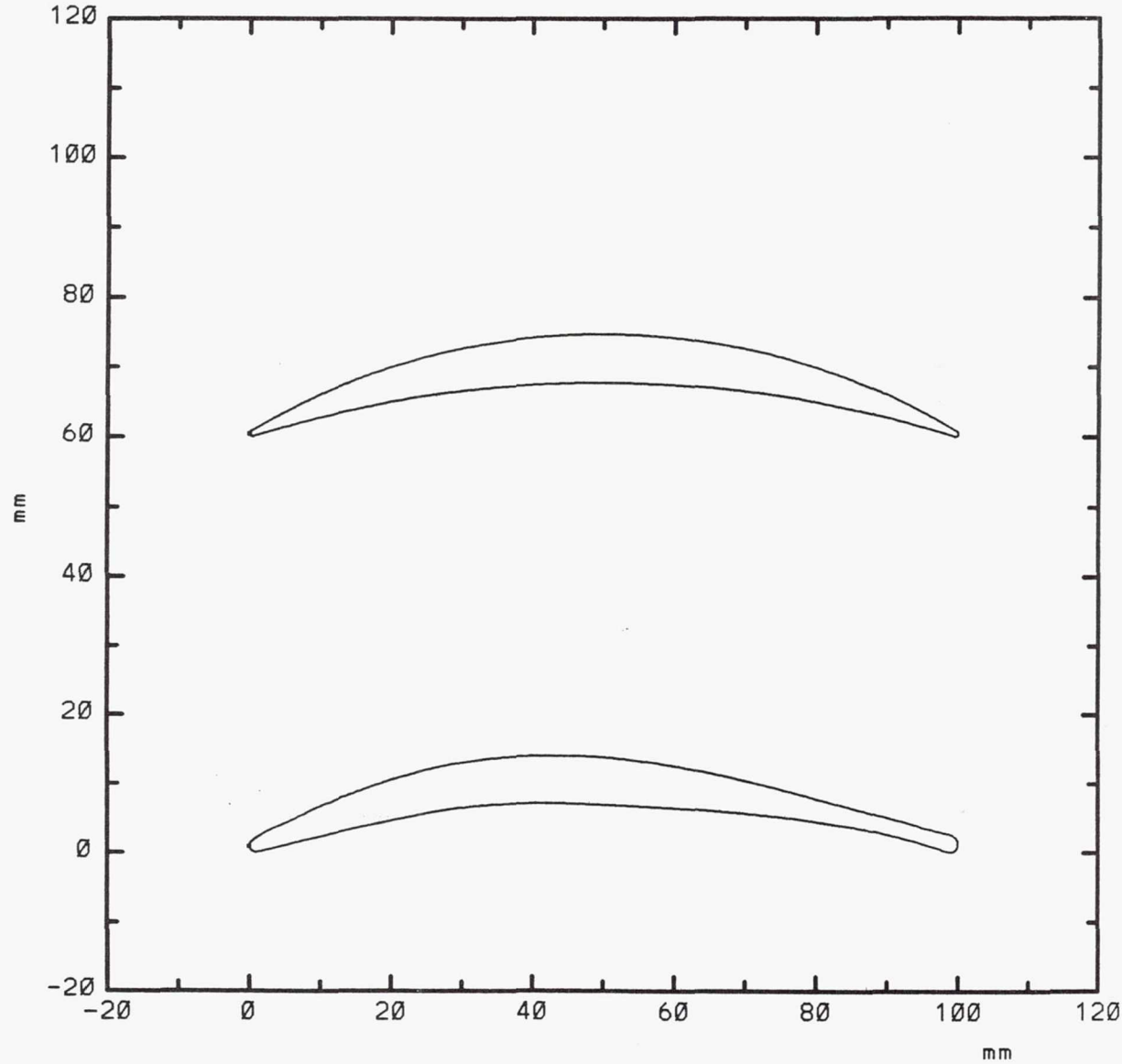

Figure 5: CD and DCA Blade Profiles.

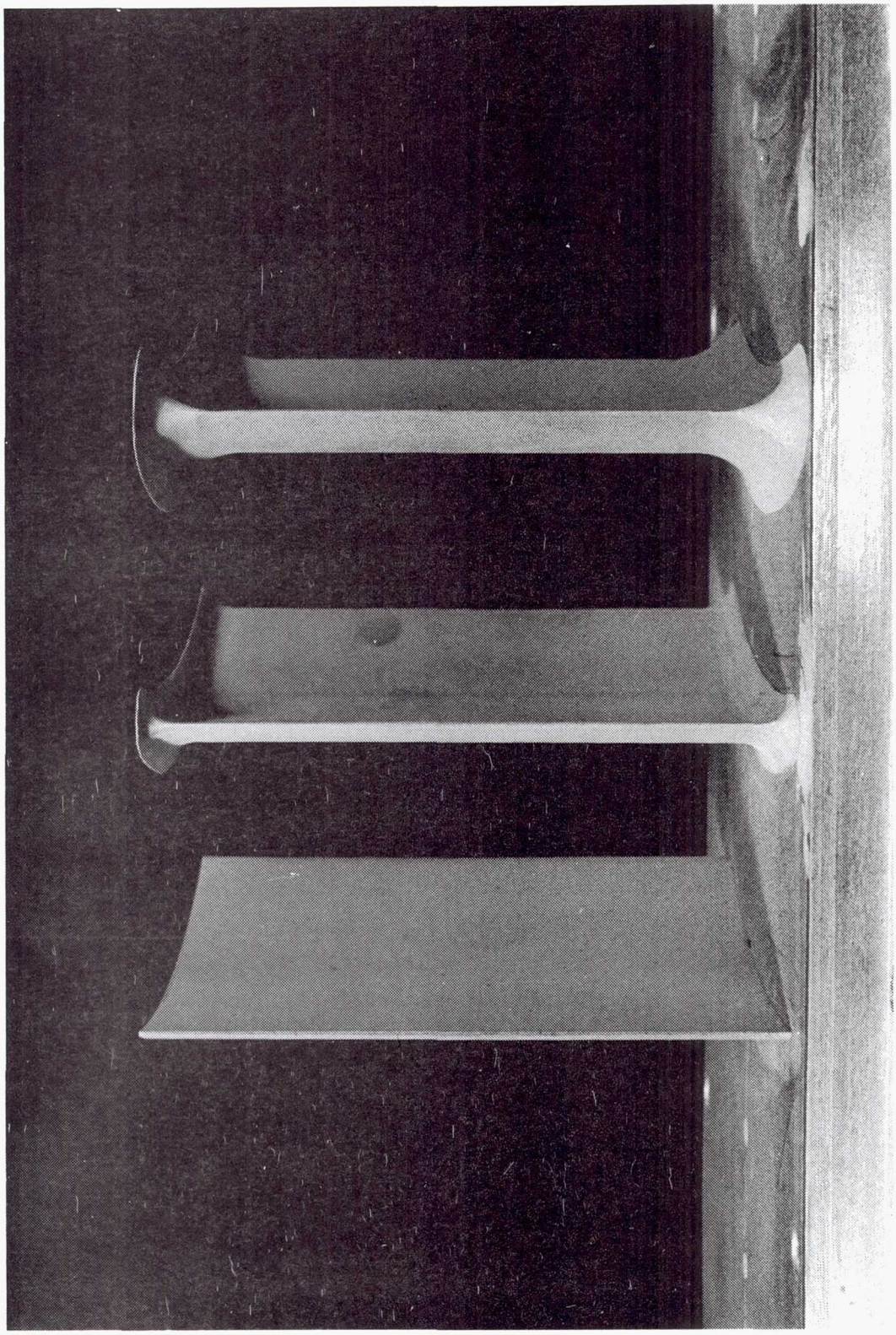

Figure 6: DCA Blades, Fillet Radii = 0, 7.5, 15.0 mm.

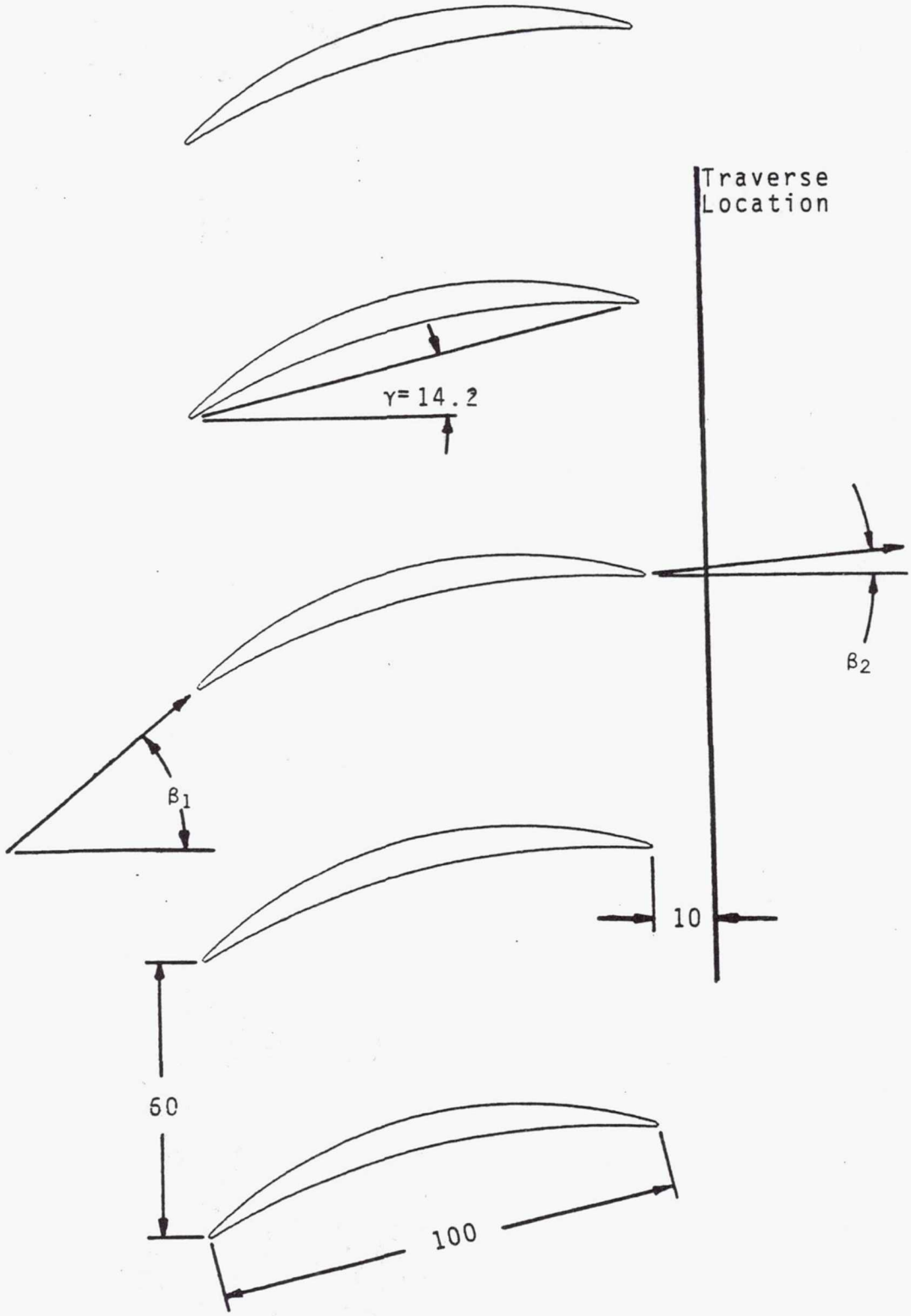

Figure 7: Cascade Geometry (dimensions in mm).

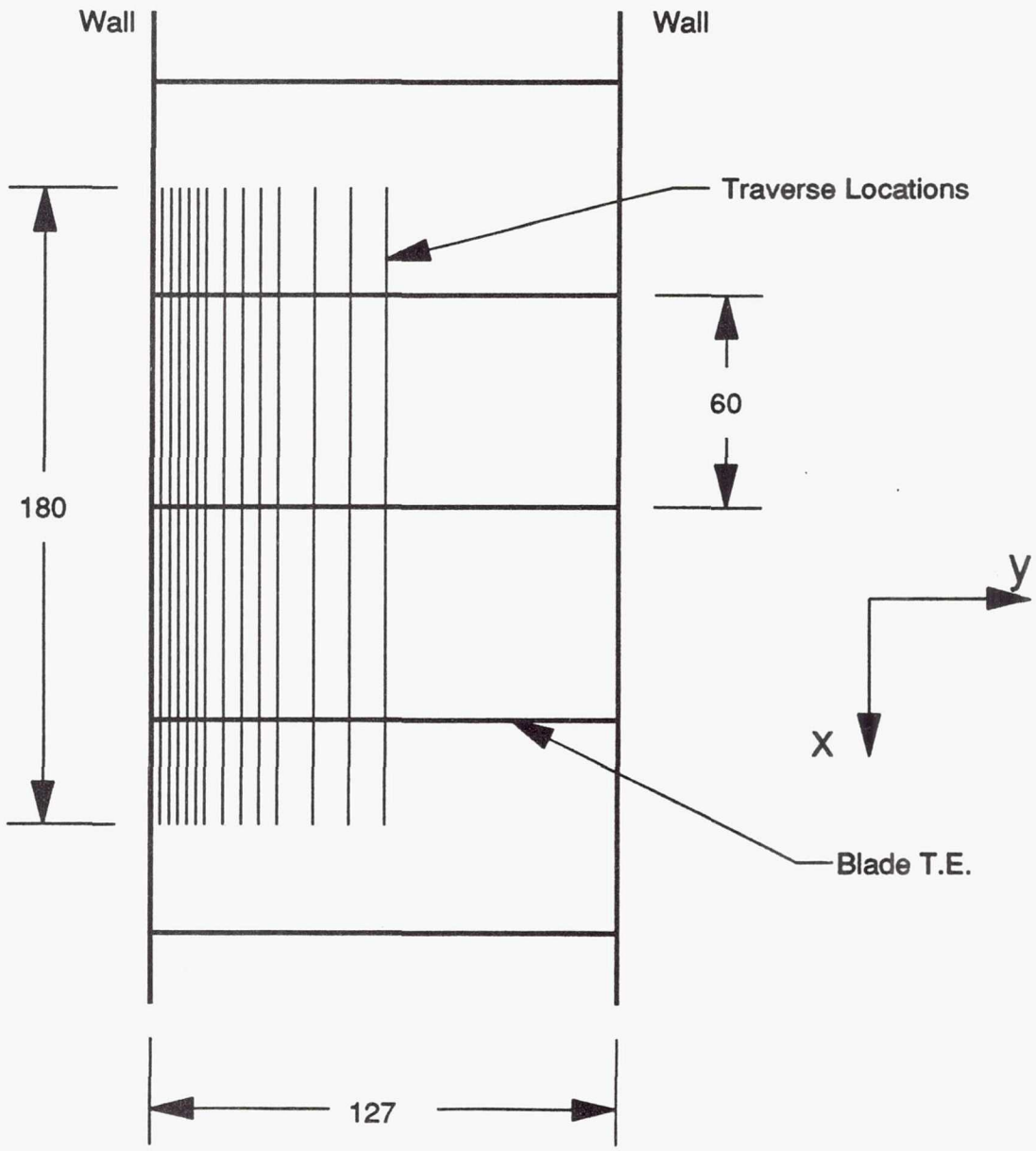

Figure 8: Traverse Locations (dimensions in mm).

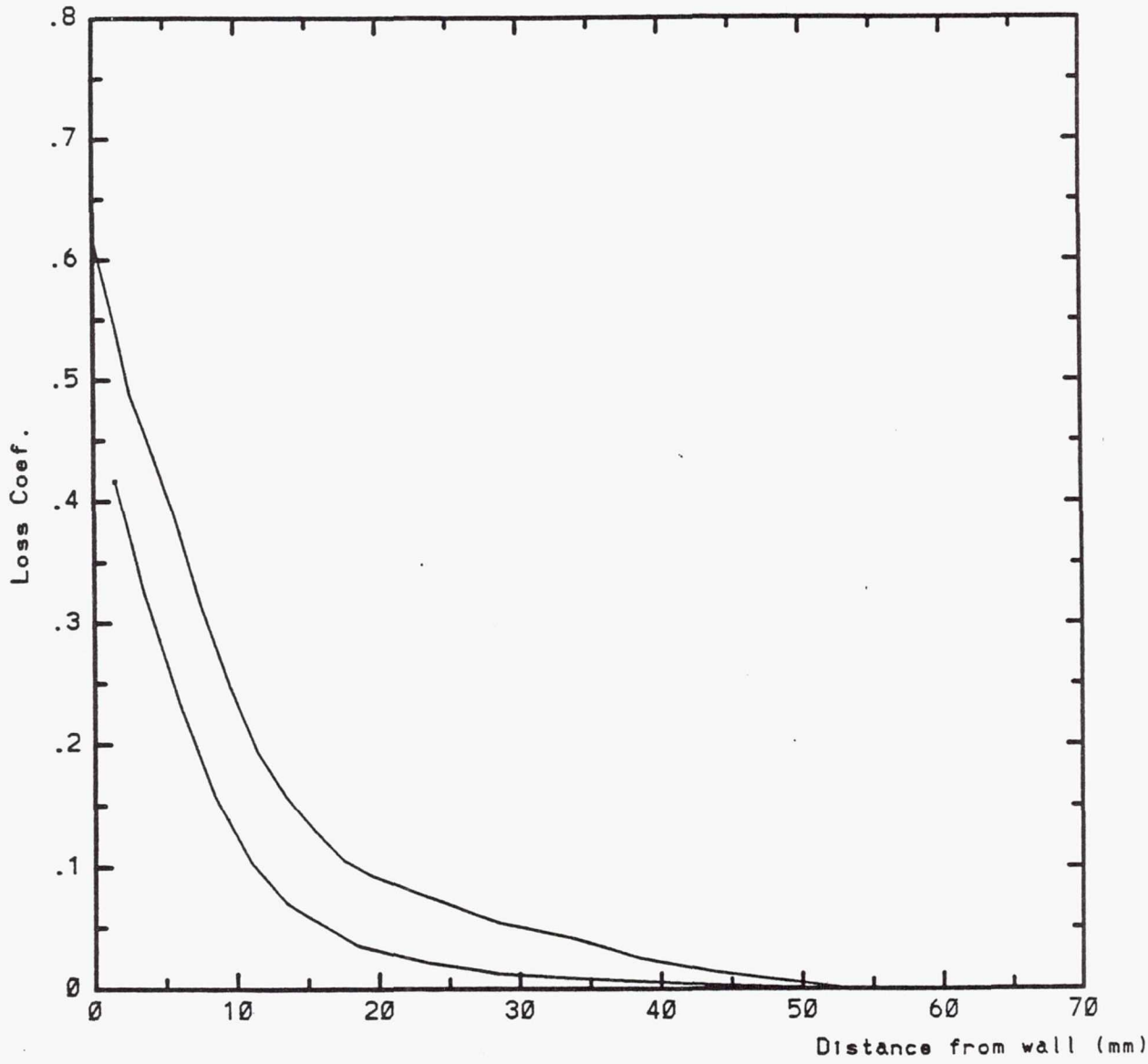

Figure 9: Boundary Layer Profiles.

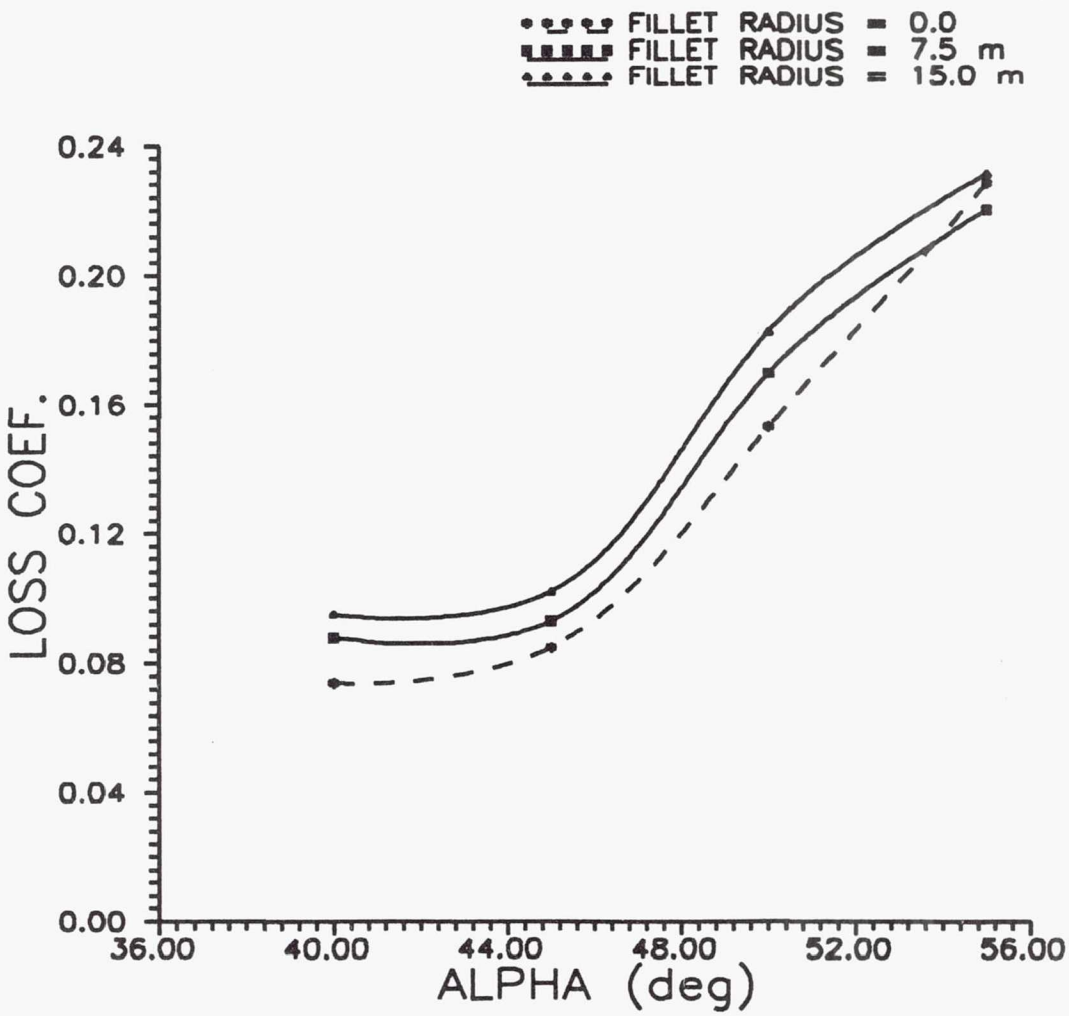

Figure 10: Total Pressure Loss Coefficient, CD Blade, BL1.

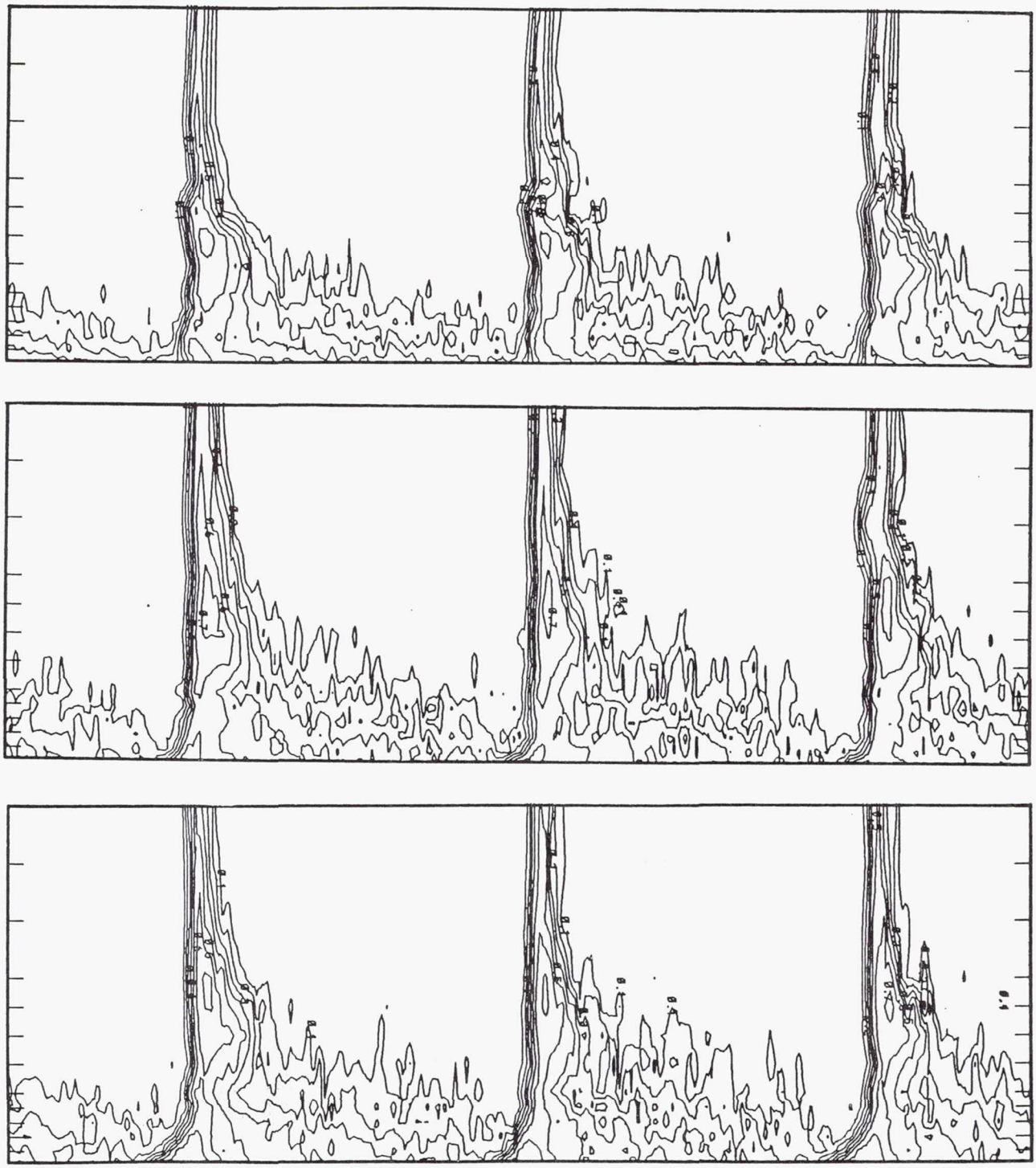

Figure 11: Loss Contour, CD Blade, BL1, α_1 = 40, (top) 0 mm fillet, (middle) 7.5 mm fillet, (bottom) 15 mm fillet.

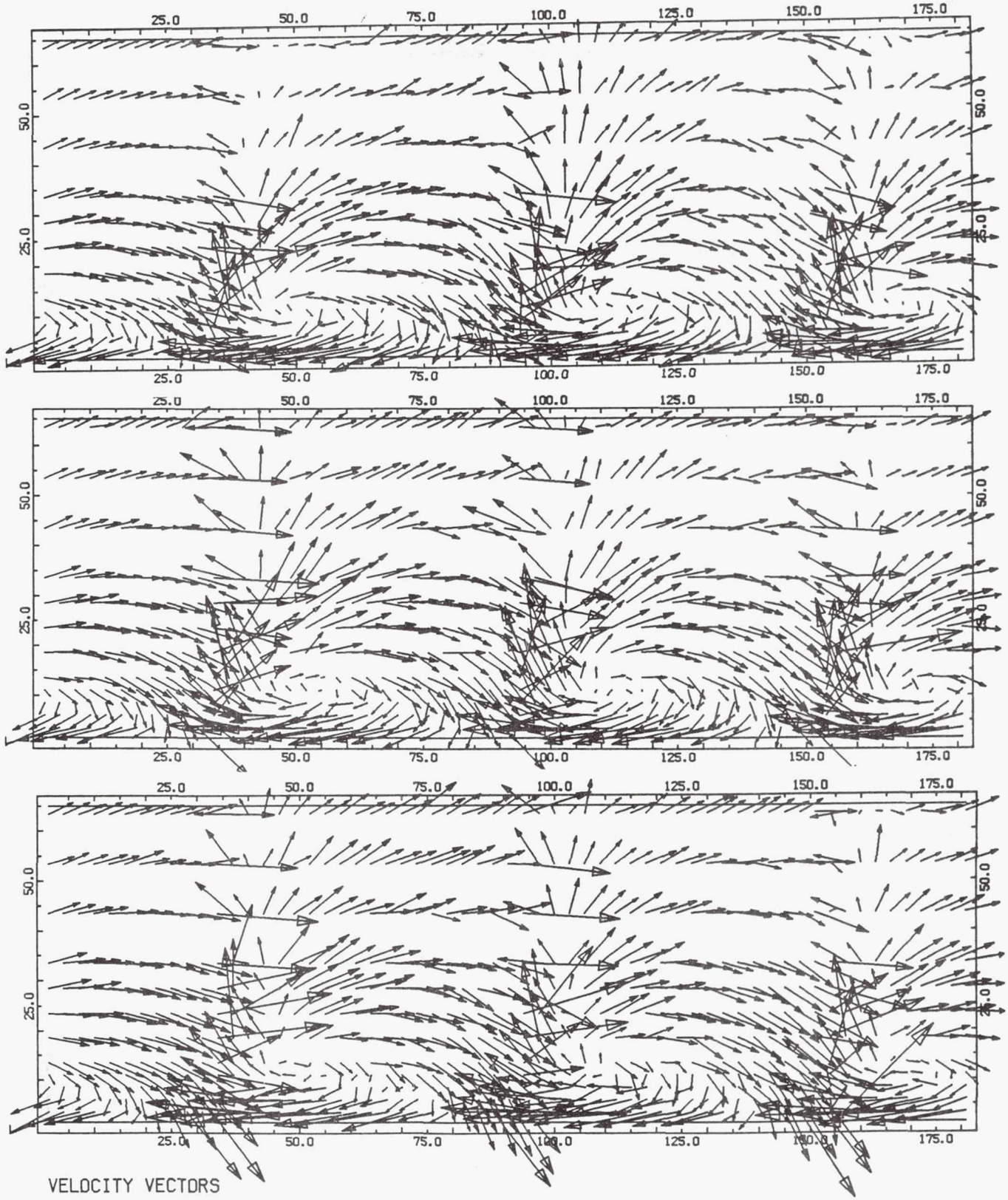

Figure 12: Velocity Vectors, CD Blade, BL1, α_1 = 40, (top) 0 mm fillet, (middle) 7.5 mm fillet, (bottom) 15 mm fillet.

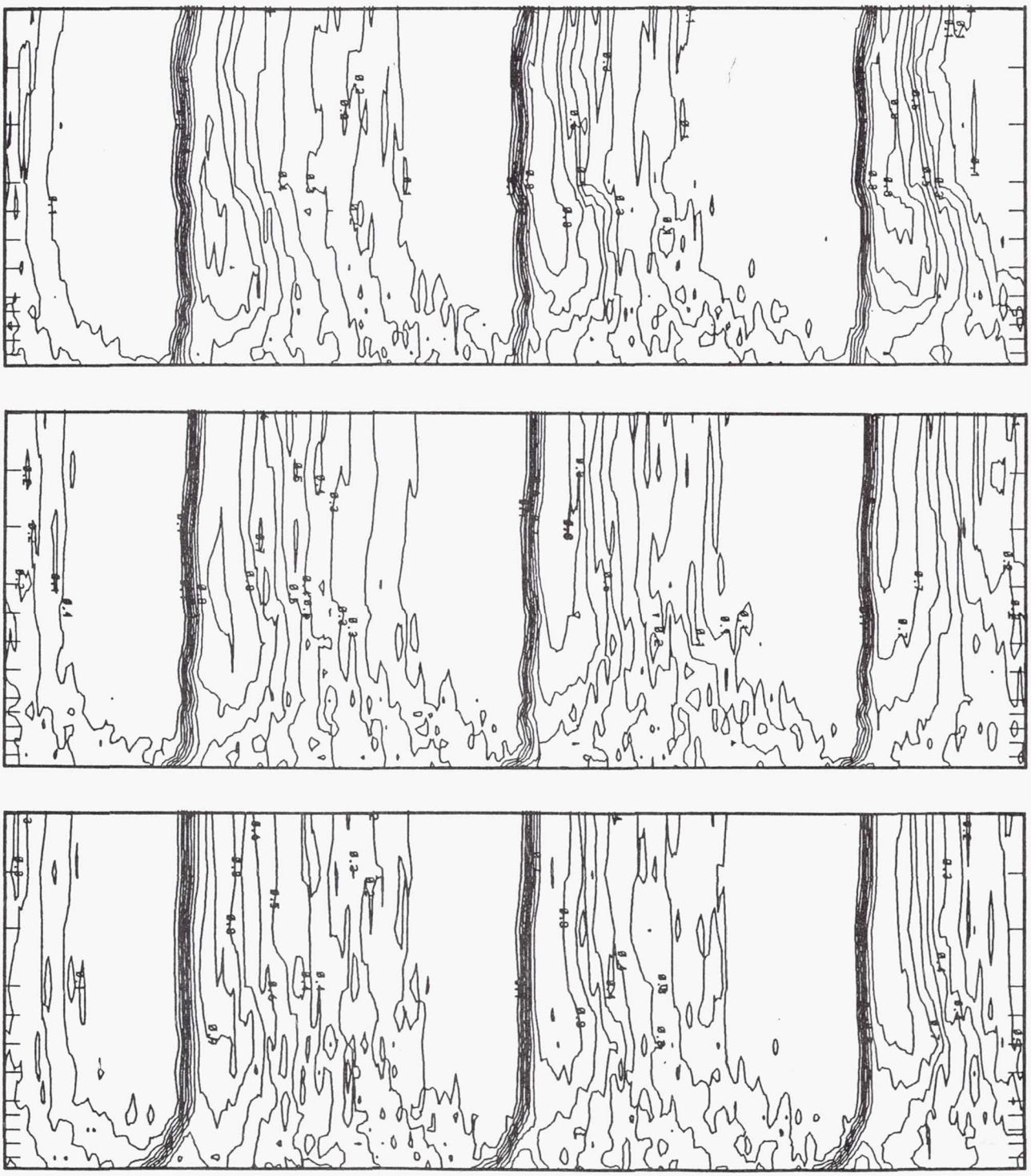

Figure 13: Loss Contour, CD Blade, BL1, α_1 = 50, (top) 0 mm fillet, (middle) 7.5 mm fillet, (bottom) 15 mm fillet.

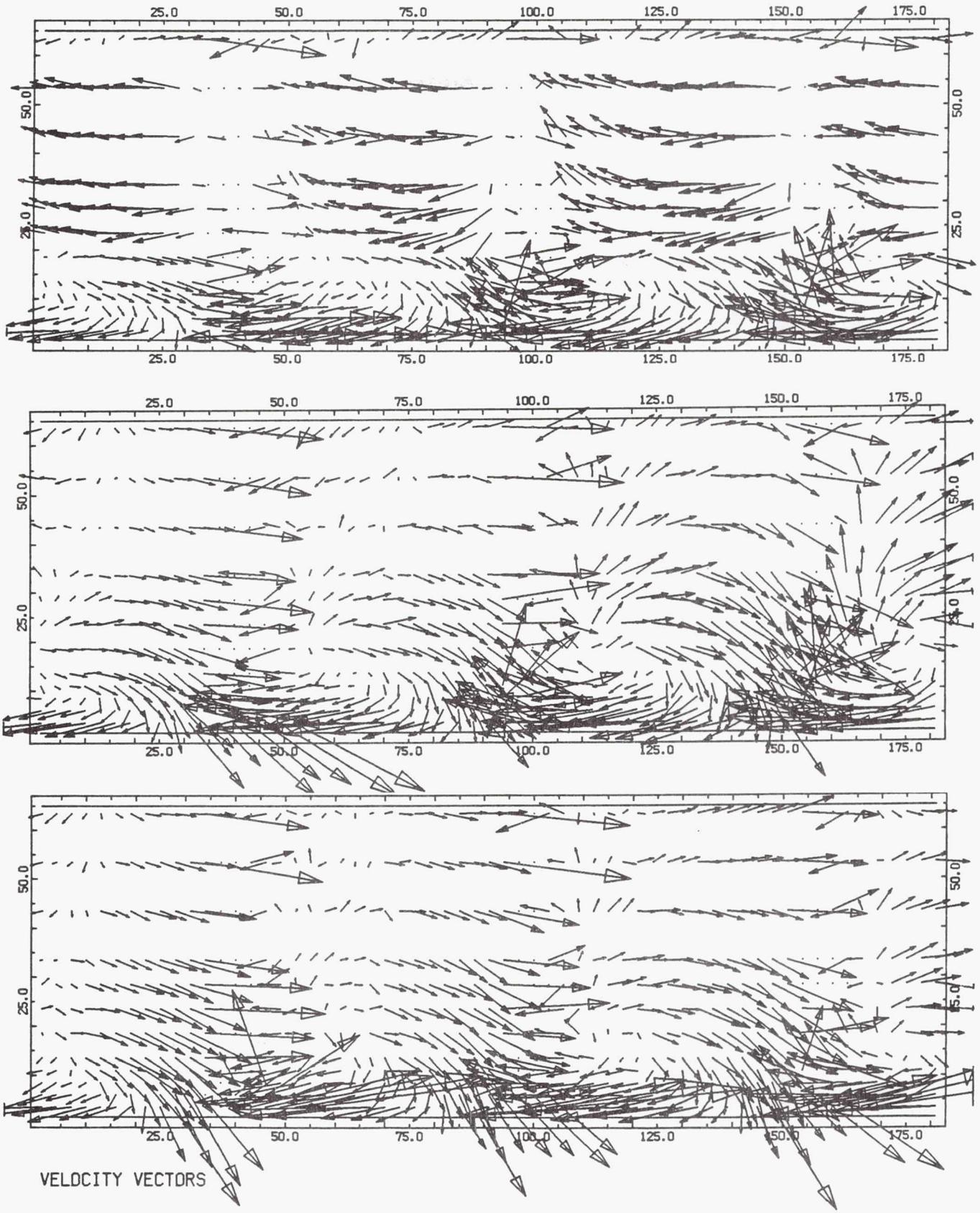

Figure 14: Velocity Vectors, CD Blade, BL1, α_1 = 50, (top) 0 mm fillet, (middle) 7.5 mm fillet, (bottom) 15 mm fillet.

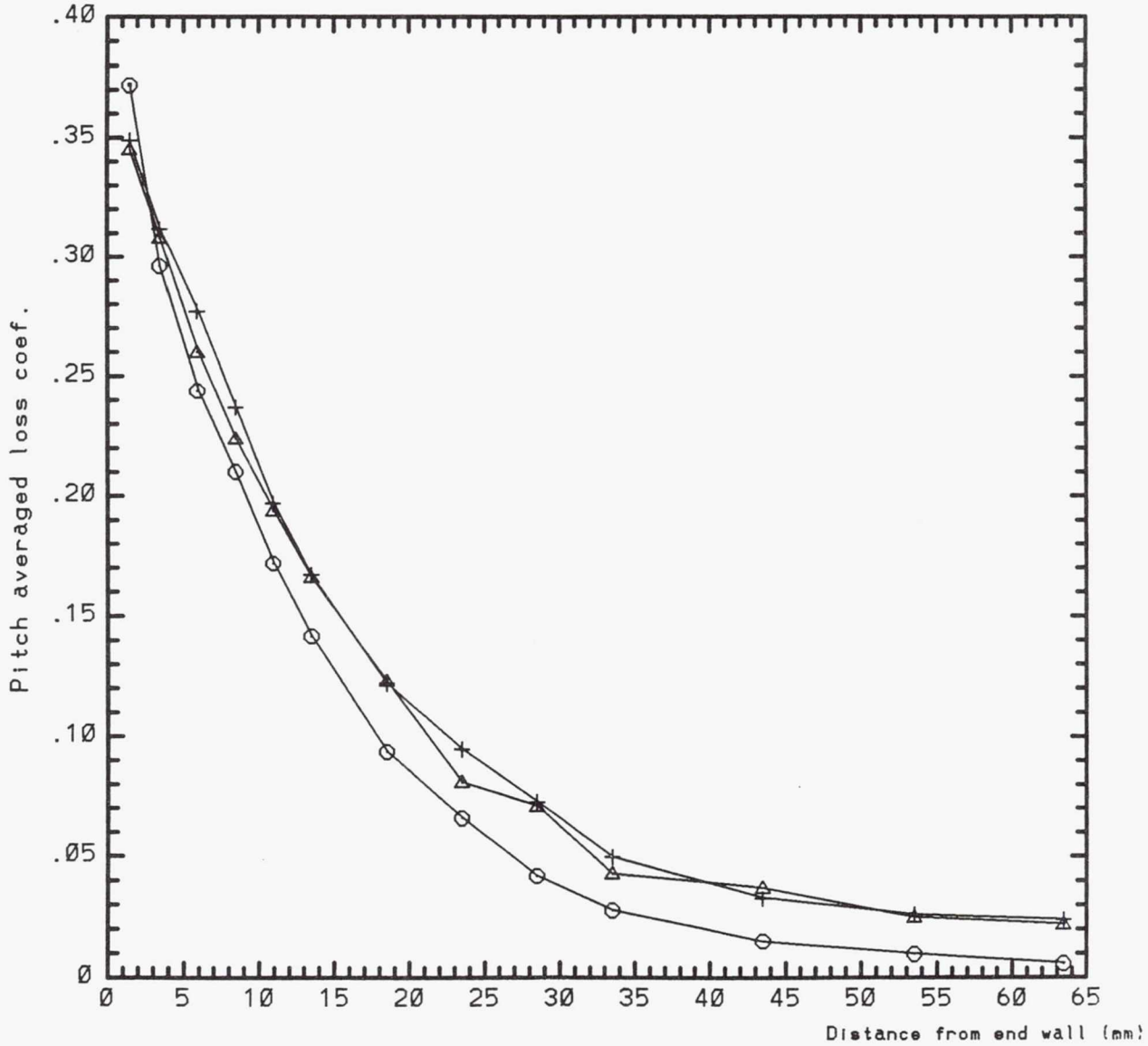

Figure 15: Spanwise Distribution of Losses, CD Blade, α_1 = 40,
BL1, o 0 mm fillet, ▵ 7.5 mm fillet, + 15 mm fillet.

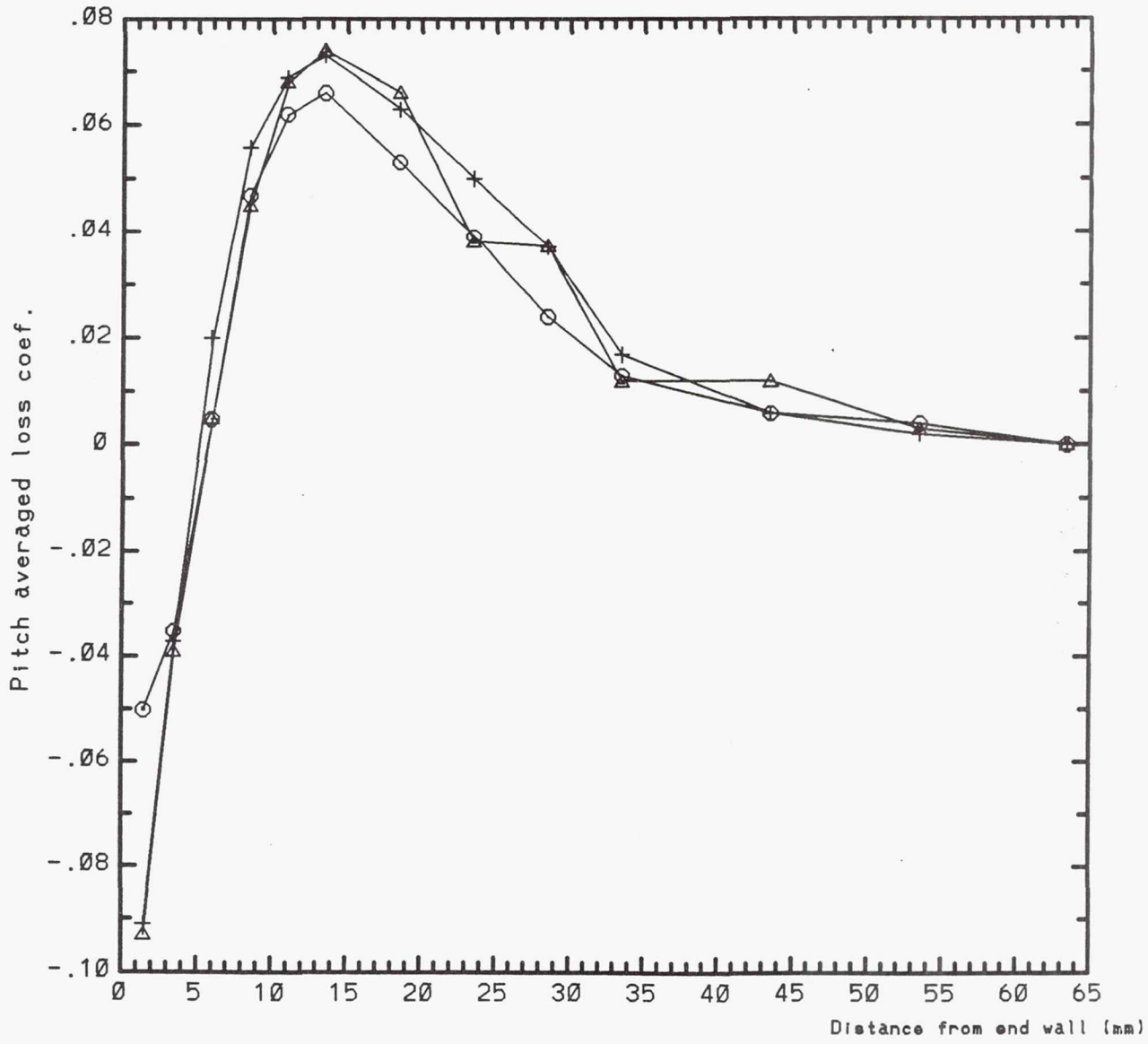

Figure 16: Spanwise Distribution of Secondary Flow Losses, CD Blade, α_1 = 40, BL1, o 0 mm fillet, Δ 7.5 mm fillet, + 15 mm fillet.

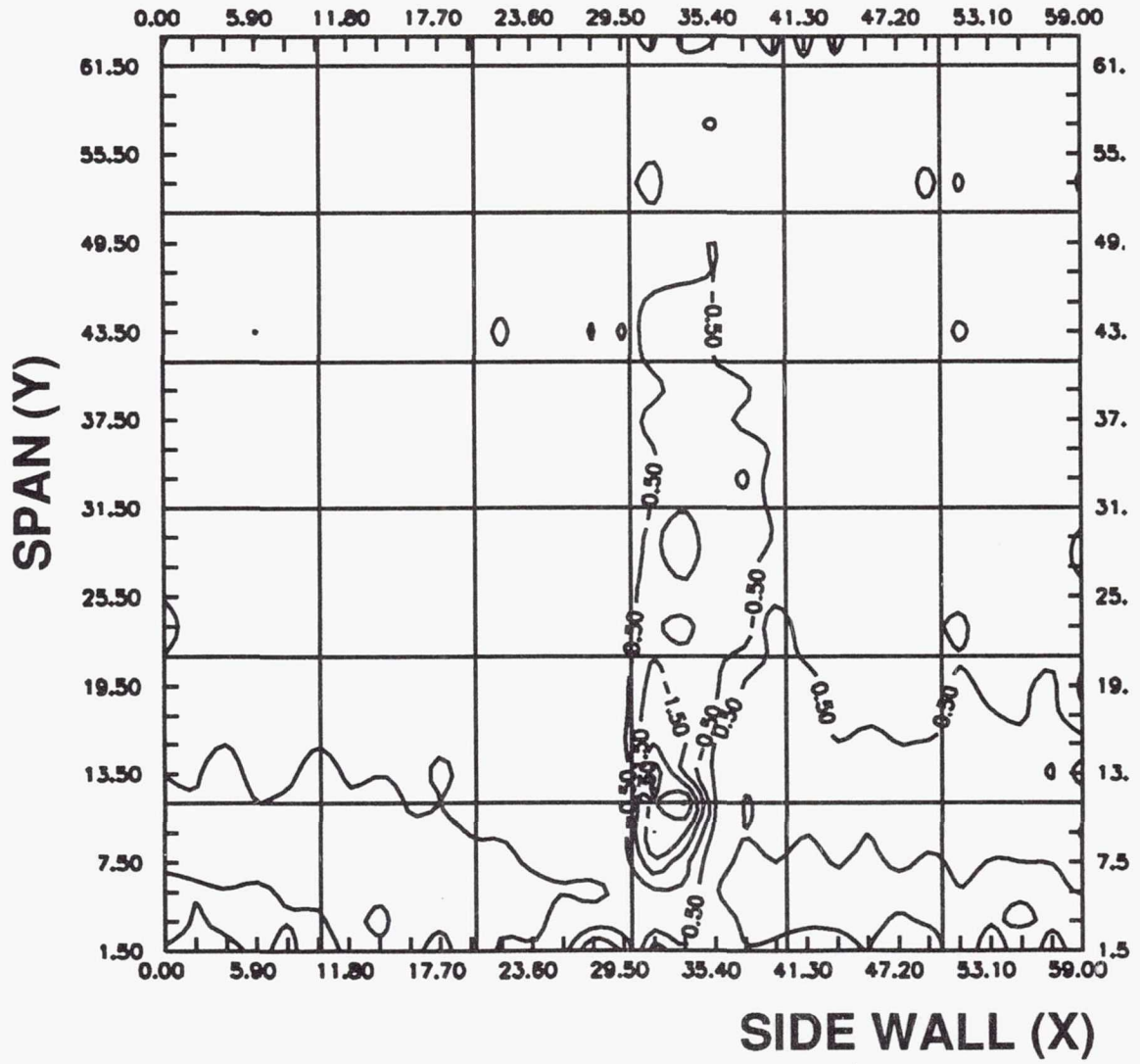

Figure 17: Streamwise Vorticity, CD Blade, α_1 = 40, BL1, Fillet Radius = 7.5 mm.

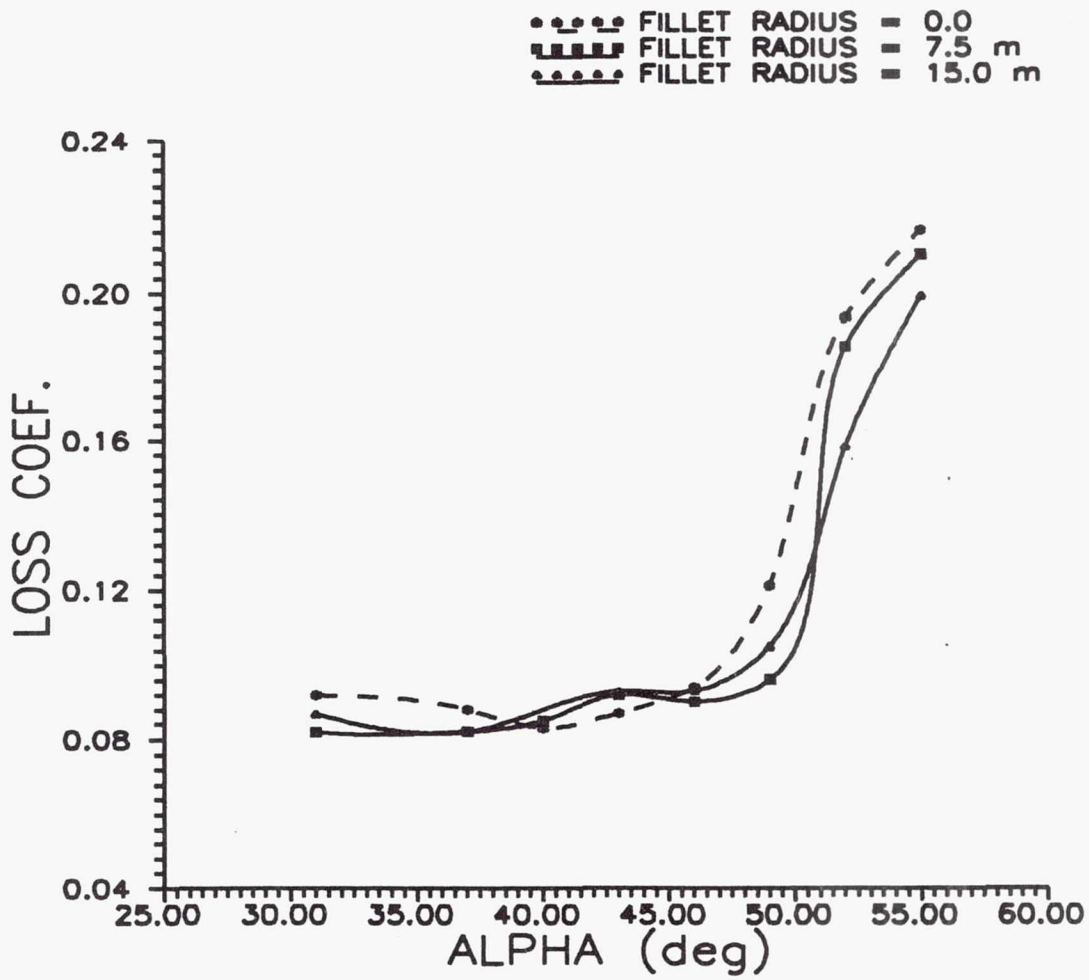

Figure 18: Total Pressure Loss Coefficient, DCA Blade, BL1.

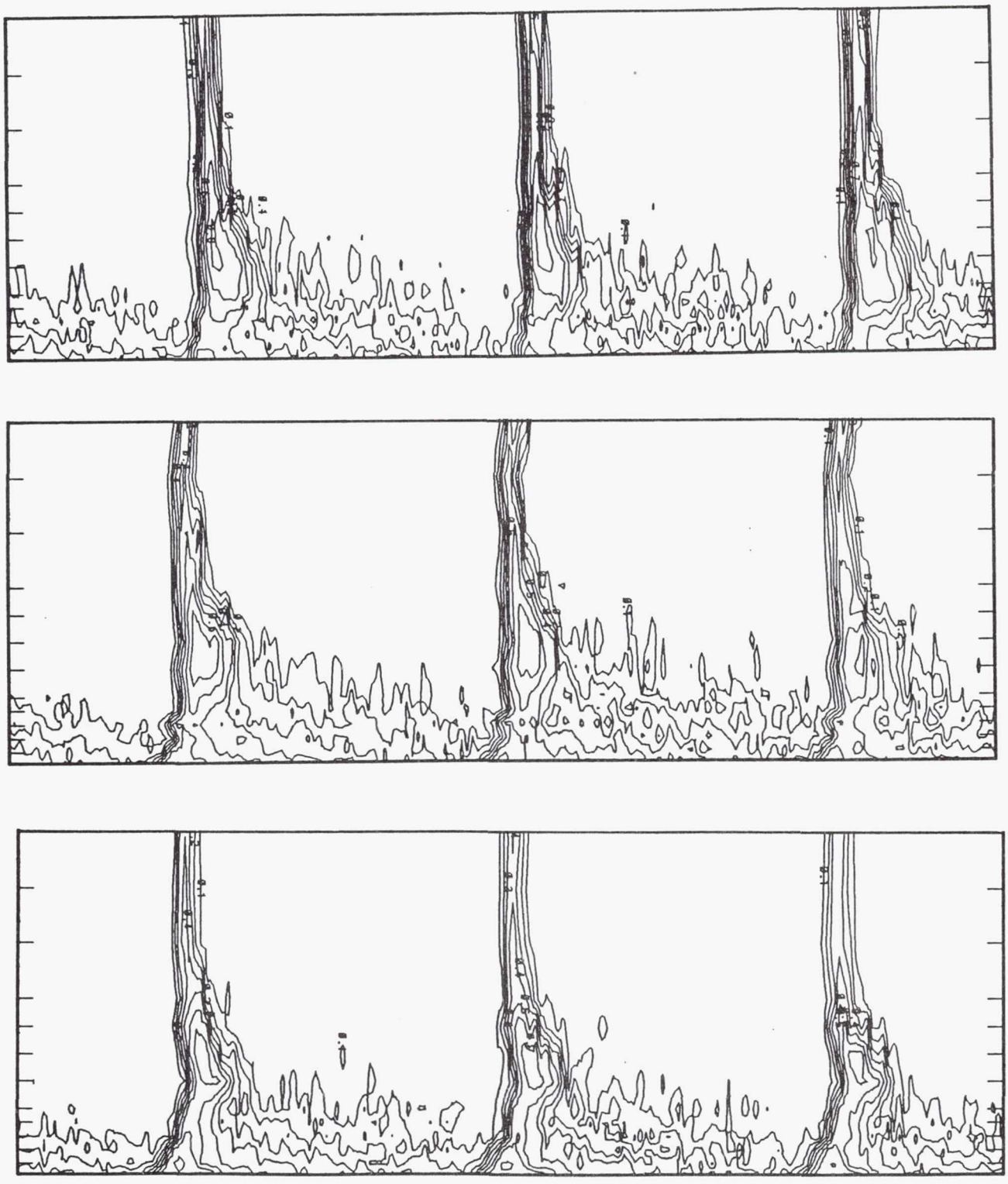

Figure 19: Loss Contour, DCA Blade, BL1, α_1 = 37, (top) 0 mm fillet, (middle) 7.5 mm fillet, (bottom) 15 mm fillet.

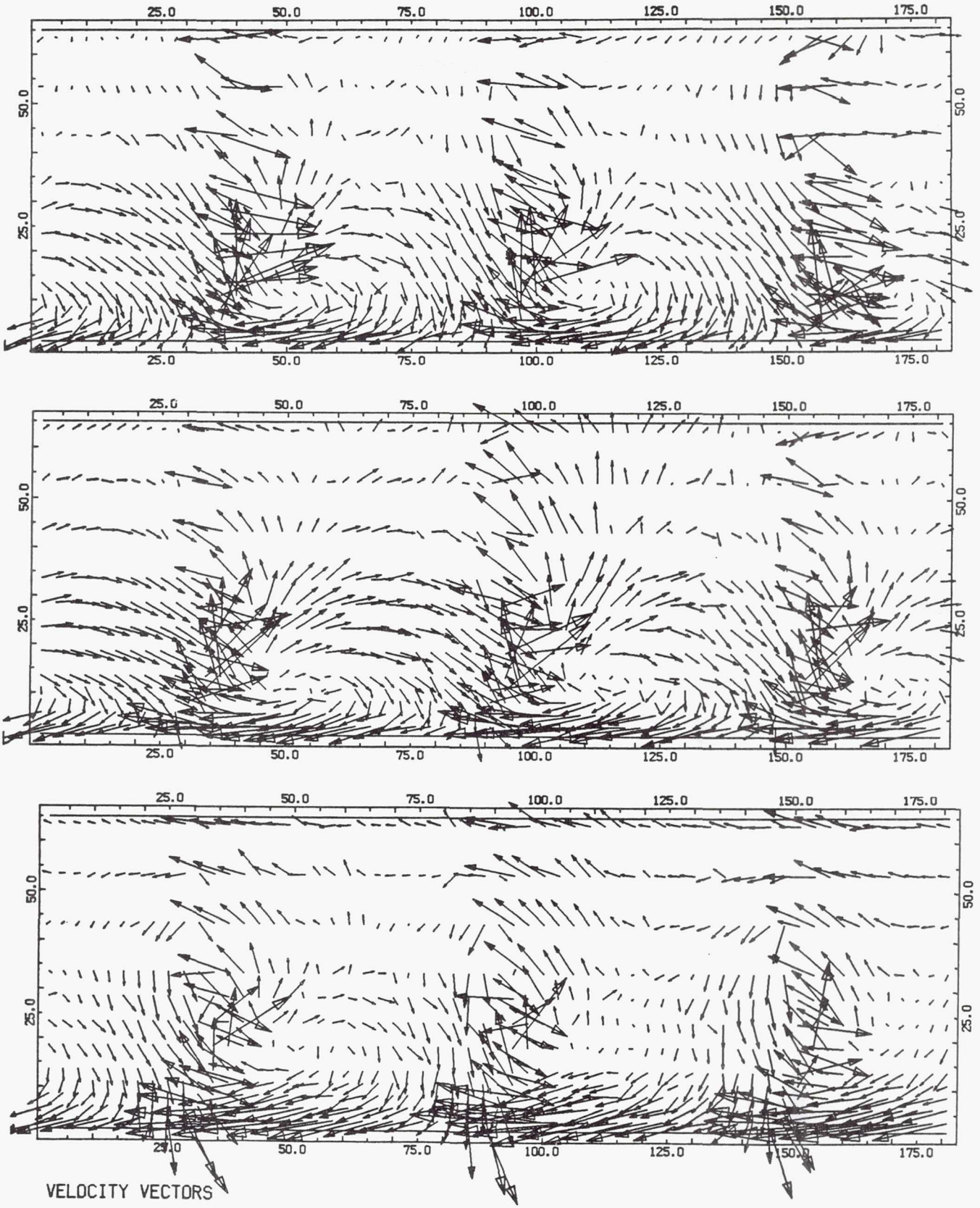

Figure 20: Velocity Vectors, DCA Blade, BL1, α_1 = 37, (top) 0 mm fillet, (middle) 7.5 mm fillet, (bottom) 15 mm fillet.

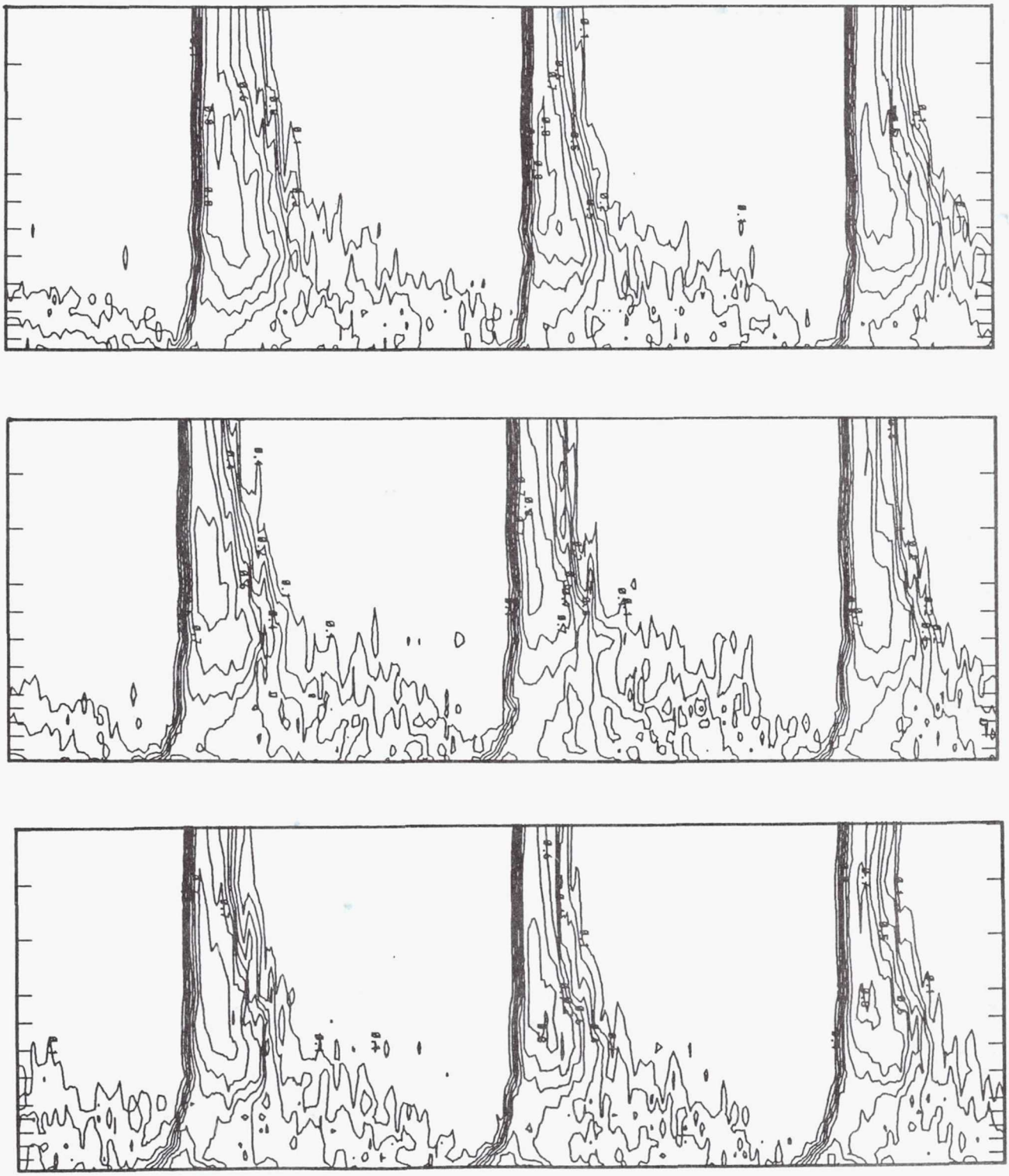

Figure 21: Loss Contour, DCA Blade, BL1, α_1 = 46, (top) 0 mm fillet, (middle) 7.5 mm fillet, (bottom) 15 mm fillet.

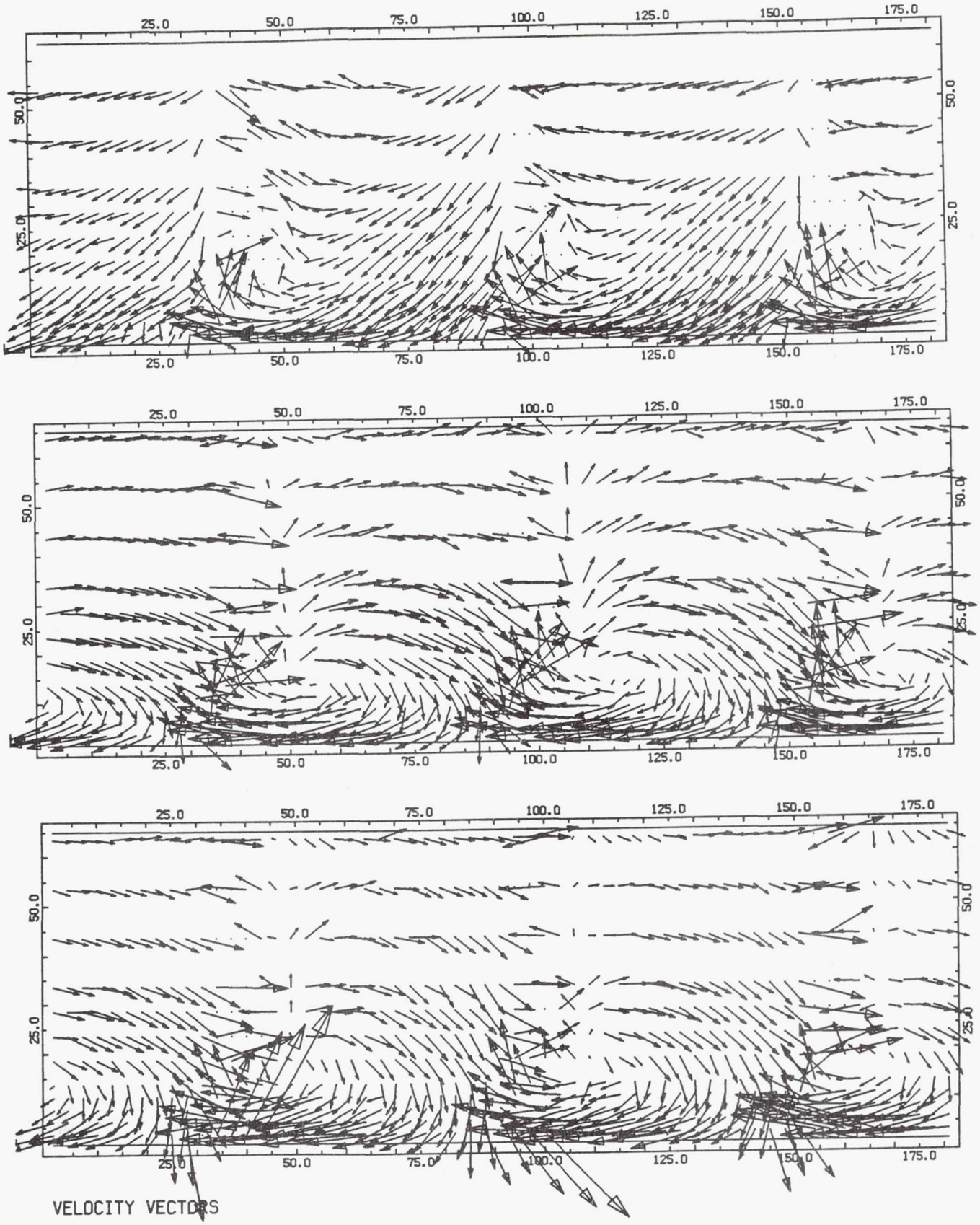

Figure 22: Velocity Vectors, DCA Blade, BL1, α_1 = 46, (top) 0 mm fillet, (middle) 7.5 mm fillet, (bottom) 15 mm fillet.

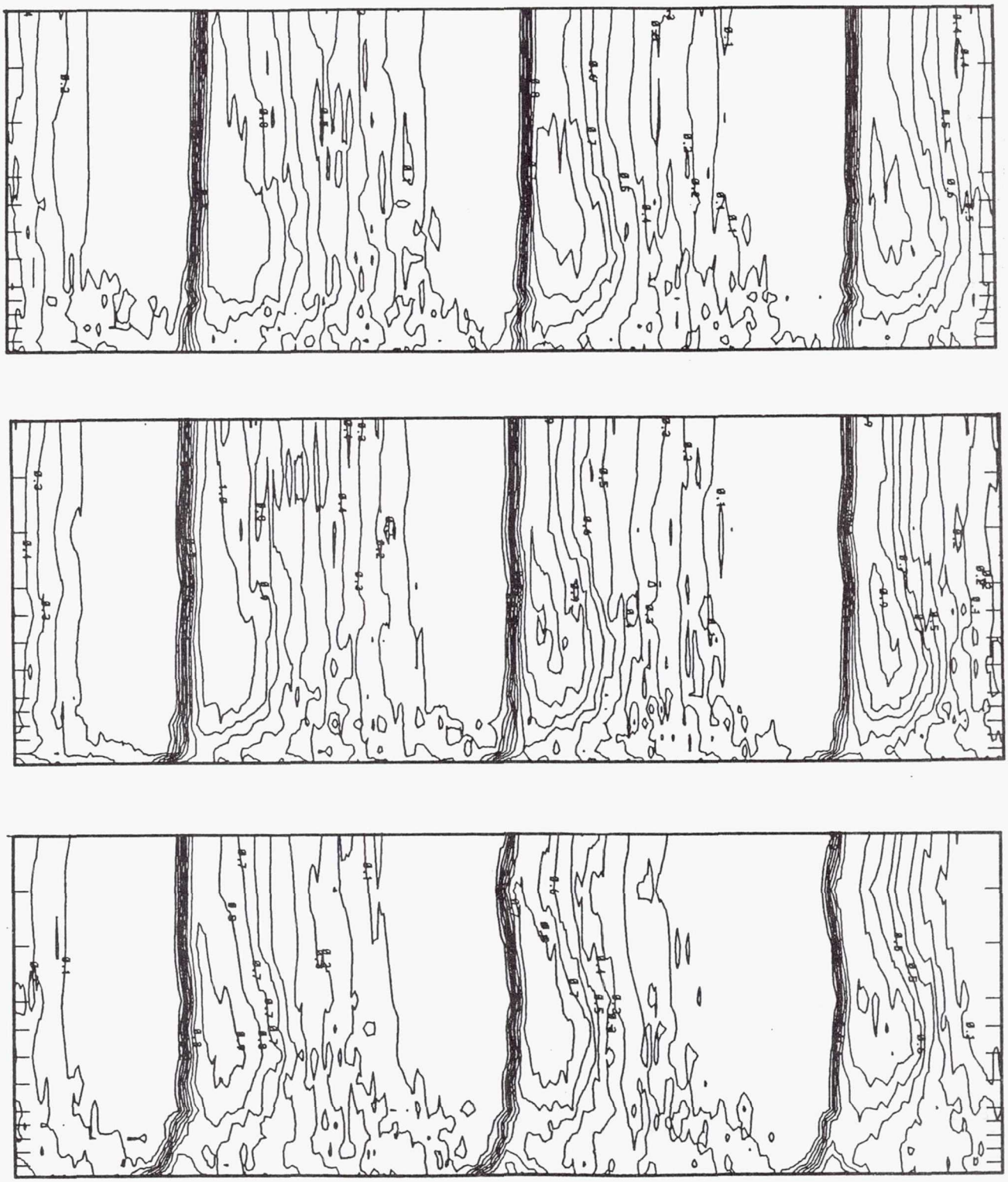

Figure 23: Loss Contour, DCA Blade, BL1, α_1 = 52, (top) 0 mm fillet, (middle) 7.5 mm fillet, (bottom) 15 mm fillet.

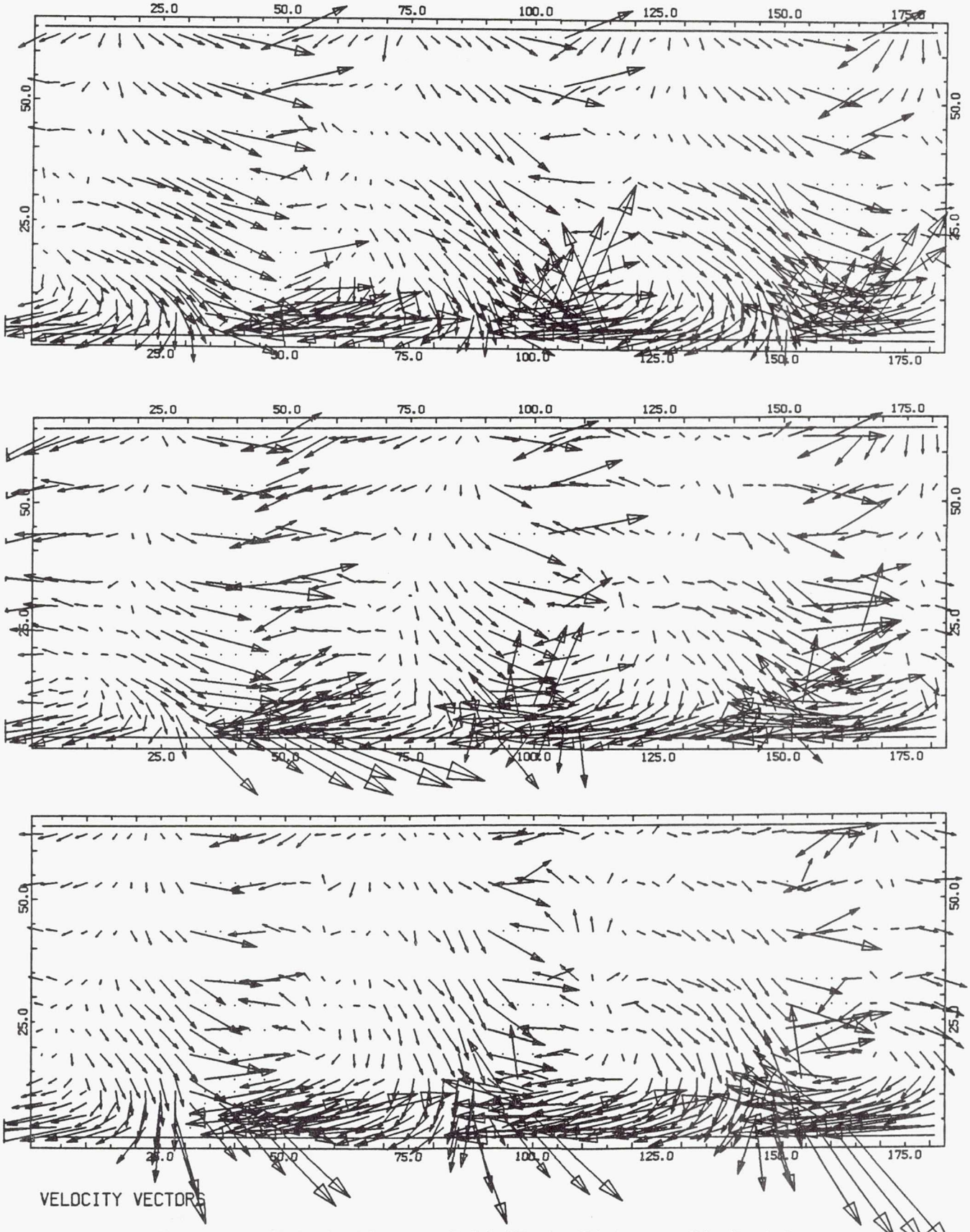

Figure 24: Velocity Vectors, DCA Blade, BL1, α_1 = 52, (top) 0 mm fillet, (middle) 7.5 mm fillet, (bottom) 15 mm fillet.

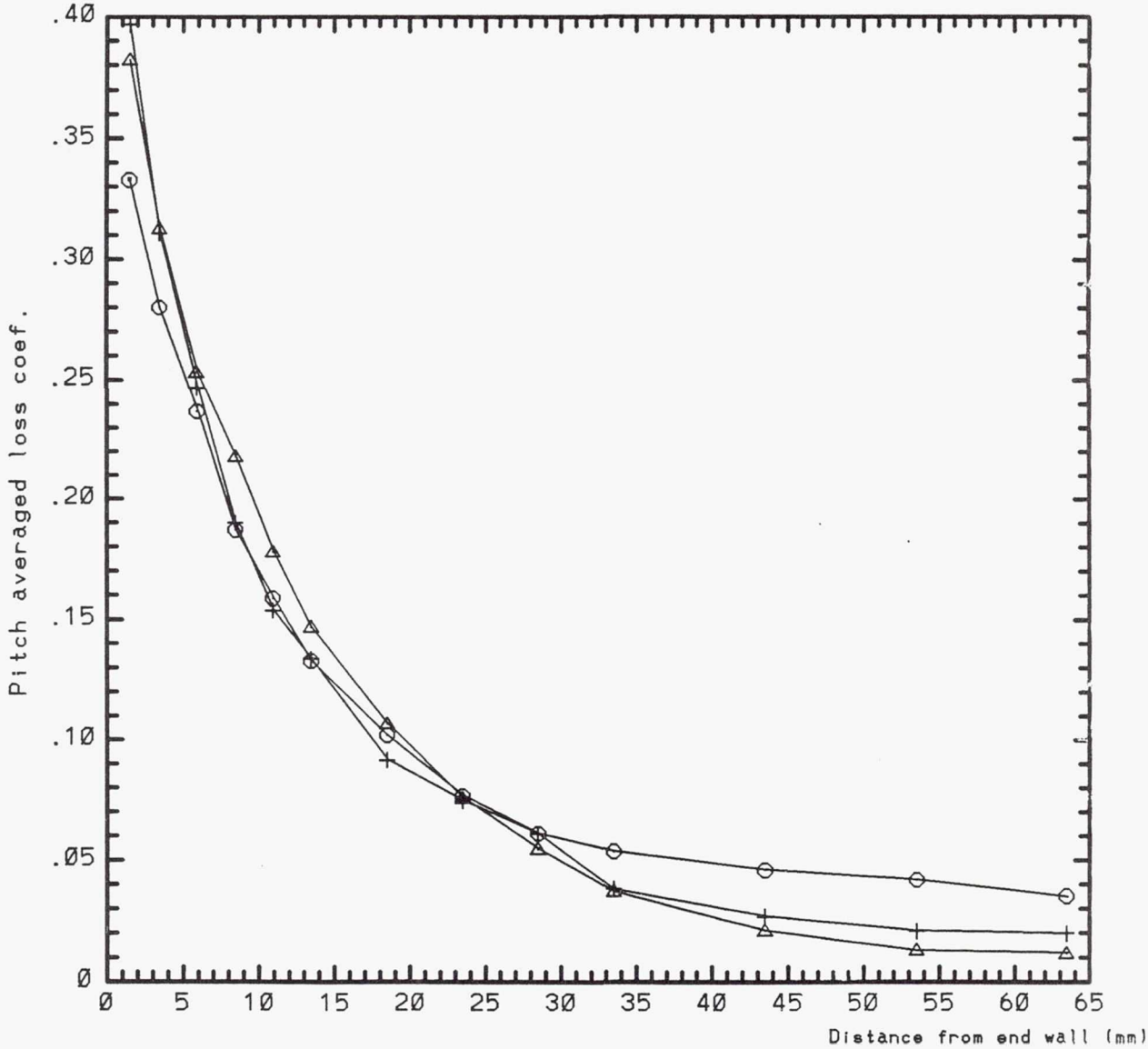

Figure 25: Spanwise Distribution of Losses, CD Blade, α_1 = 40, BL1, o 0 mm fillet, Δ 7.5 mm fillet, + 15 mm fillet.

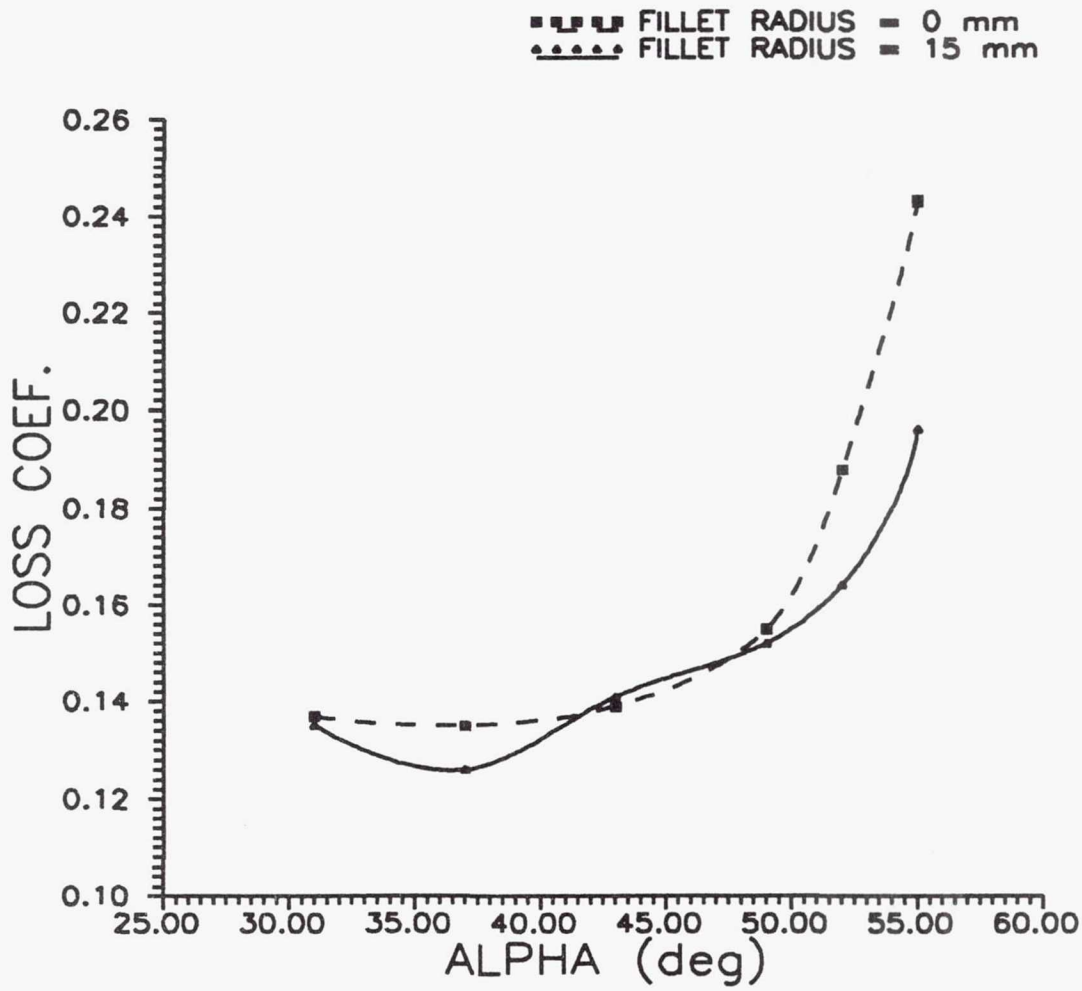

Figure 26: Total Pressure Loss Coefficient, DCA Blade, BL2.

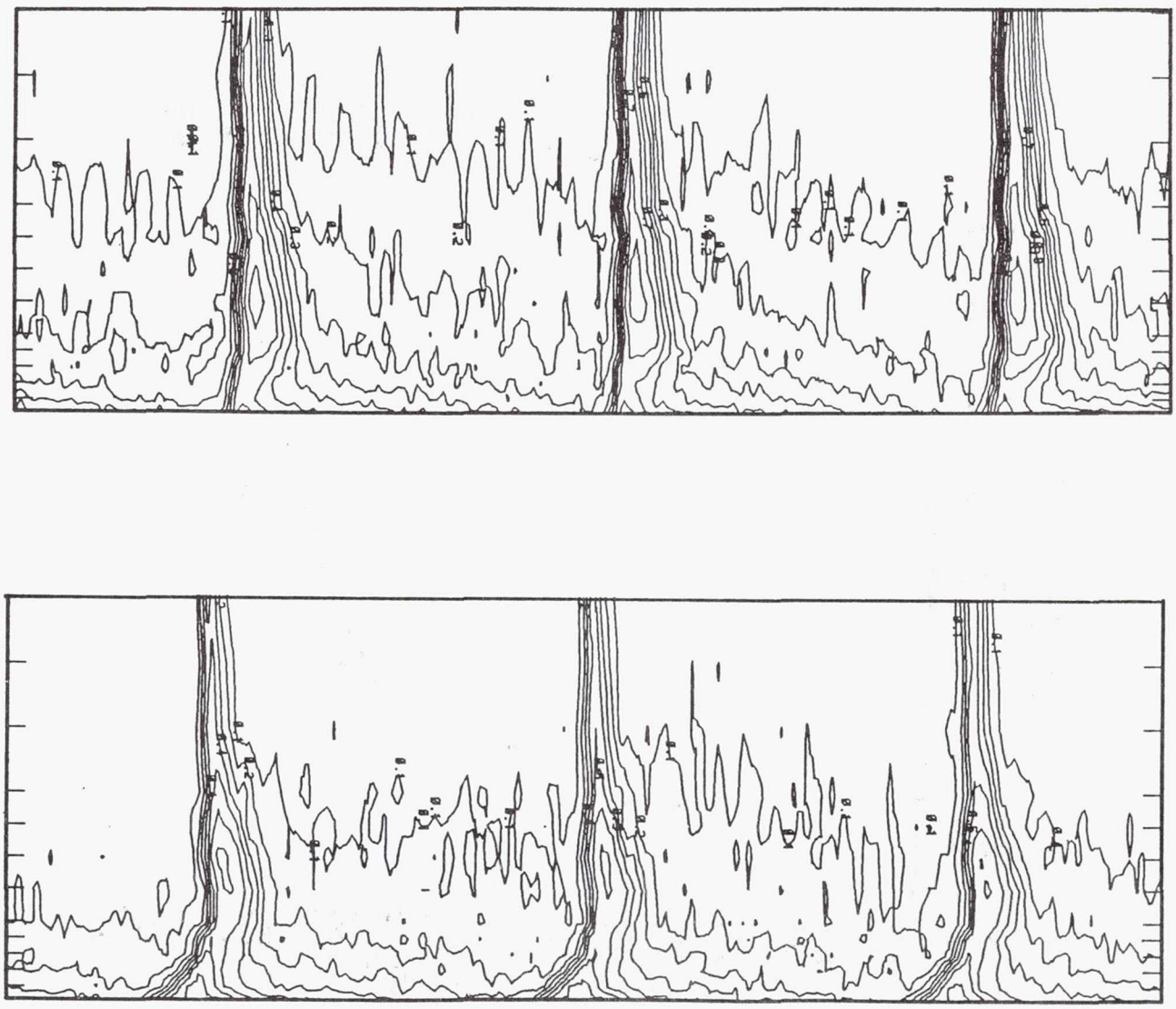

Figure 27: Loss Contour, DCA Blade, BL2, α_1 = 37, (top) 0 mm fillet, (bottom) 15 mm fillet.

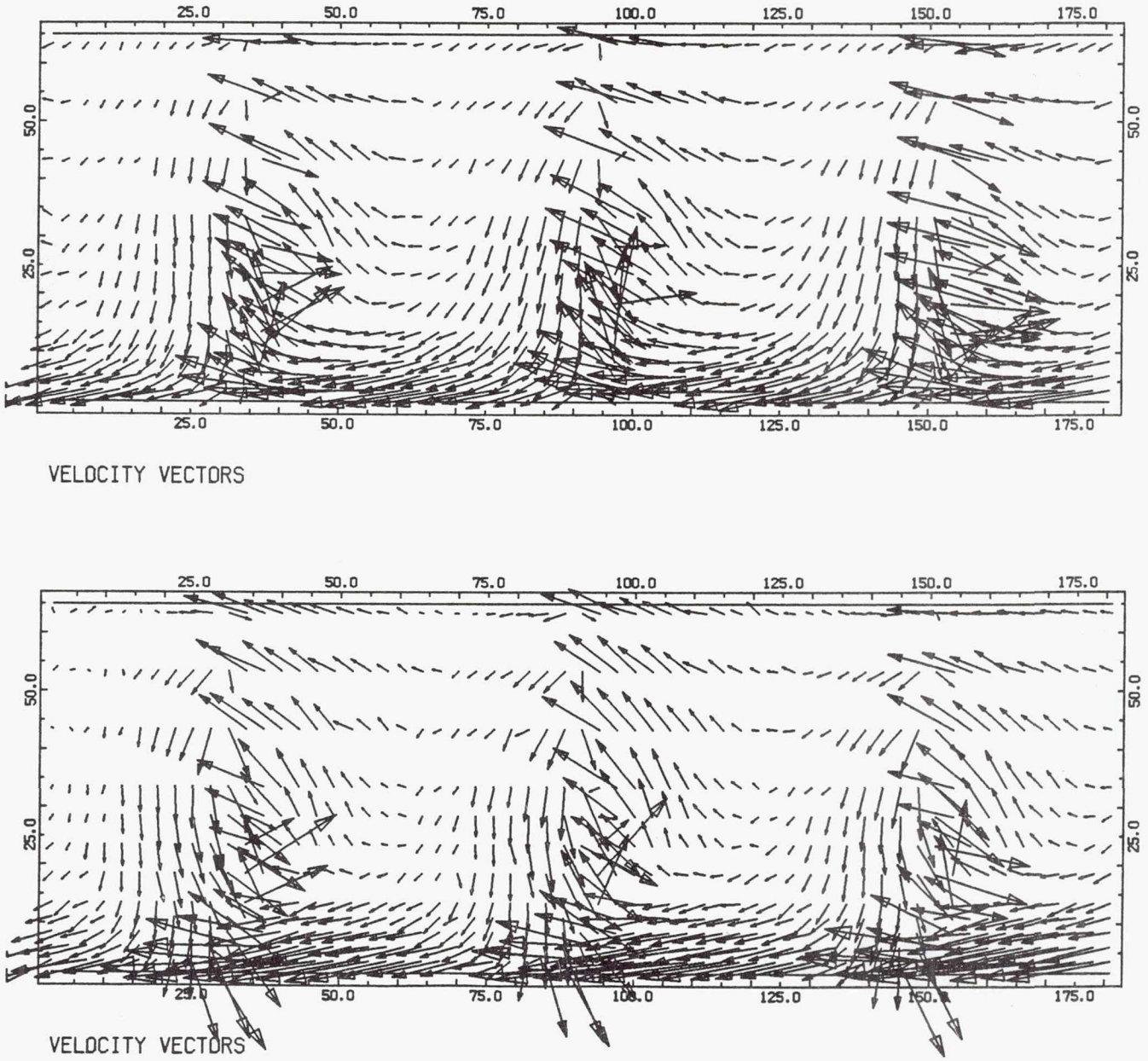

Figure 28: Velocity Vectors, DCA Blade, BL2, α_1 = 37, (top) 0 mm fillet, (bottom) 15 mm fillet.

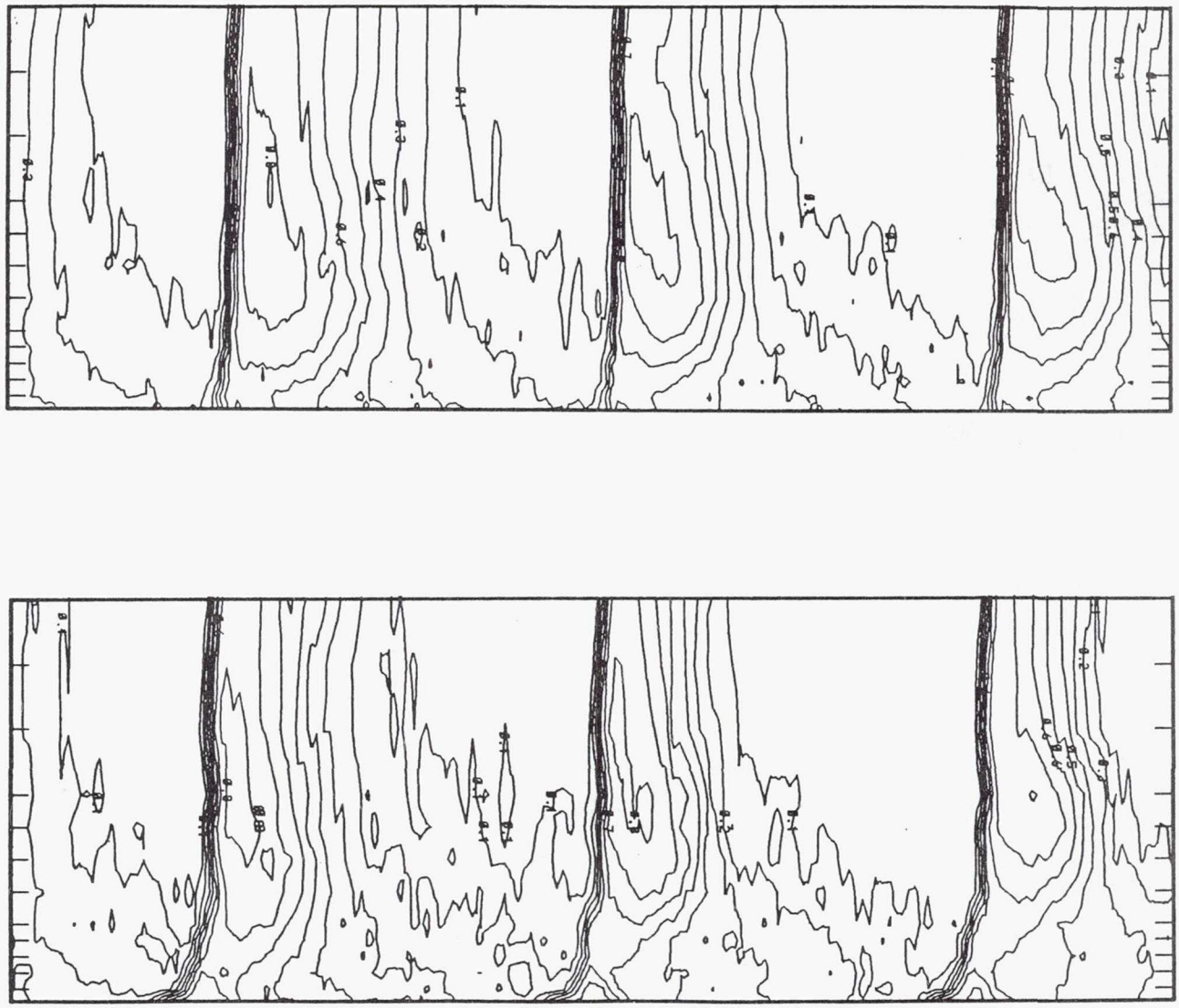

Figure 29: Loss Contour, DCA Blade, BL2, α_1 = 52, (top) 0 mm fillet, (bottom) 15 mm fillet.

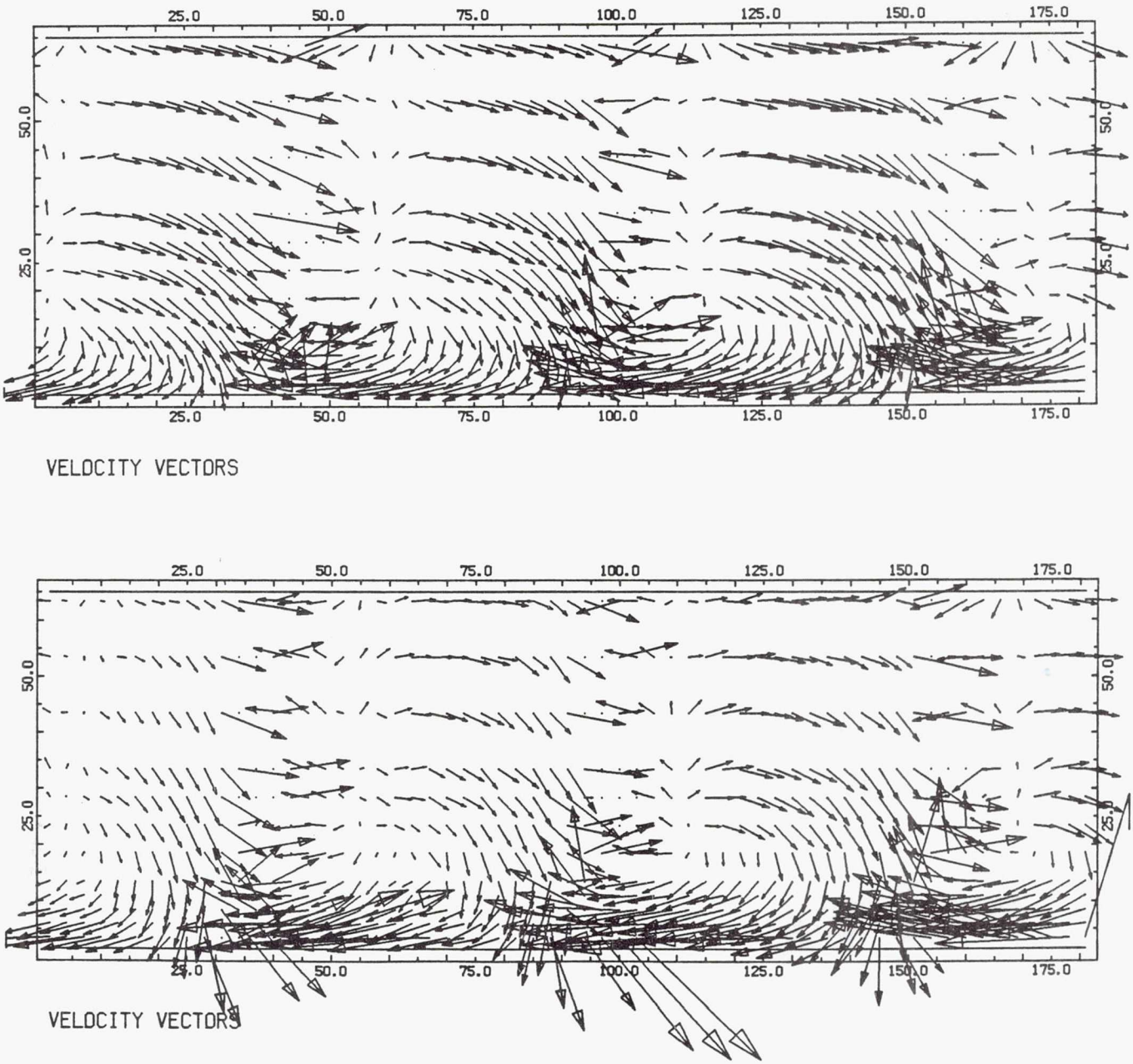

Figure 30: Velocity Vectors, DCA Blade, BL2, α_1 = 52, (top) 0 mm fillet, (bottom) 15 mm fillet.

REPORT DOCUMENTATION PAGE

Form Approved
OMB No. 0704-0188

1. AGENCY USE ONLY (*Leave blank*)	2. REPORT DATE	3. REPORT TYPE AND DATES COVERED
	November 1991	Technical Memorandum

4. TITLE AND SUBTITLE

The Aerodynamic Effect of Fillet Radius in a Low Speed Compressor Cascade

5. FUNDING NUMBERS

WU-505-69-10

6. AUTHOR(S)

Brian P. Curlett

7. PERFORMING ORGANIZATION NAME(S) AND ADDRESS(ES)

National Aeronautics and Space Administration
Lewis Research Center
Cleveland, Ohio 44135-3191

8. PERFORMING ORGANIZATION REPORT NUMBER

E-6717

9. SPONSORING/MONITORING AGENCY NAMES(S) AND ADDRESS(ES)

National Aeronautics and Space Administration
Washington, D.C. 20546-0001

10. SPONSORING/MONITORING AGENCY REPORT NUMBER

NASA TM-105347

11. SUPPLEMENTARY NOTES

Report was submitted in fulfillment of the requirements of the Diploma Course at the von Karman Institute for Fluid Dynamics, Belgium.

12a. DISTRIBUTION/AVAILABILITY STATEMENT

Unclassified - Unlimited
Subject Category 07

12b. DISTRIBUTION CODE

13. ABSTRACT ***(Maximum 200 words)***

The aerodynamic effects of fillet size in a low speed compressor cascade were investigated experimentally. Two blade profiles were used during the experiment, namely a controlled diffusion blade and a double circular arc blade. Cascades were tested with three fillet radii and two boundary layer thicknesses over a large range of incidence angles. The cascade performance was determined by extensive downstream flow measurements using a two head, 5-hole pressure probe. Results differ significantly between the two types of blades tested. As fillet radius increases secondary flows and total pressure losses were found to increase for the controlled diffusion blades; whereas, for the double circular arc blades the losses decrease, particularly at high incidence angles.

14. SUBJECT TERMS

Compressors; Cascade flow; Fillets

15. NUMBER OF PAGES

48

16. PRICE CODE

A03

17. SECURITY CLASSIFICATION OF REPORT	18. SECURITY CLASSIFICATION OF THIS PAGE	19. SECURITY CLASSIFICATION OF ABSTRACT	20. LIMITATION OF ABSTRACT
Unclassified	Unclassified	Unclassified	